Green Synthesis of Magnetite Nanoparticles Using *Catha Edulis* Plant Leaf Extract for Removal of Hexavalent Chromium from Aqueous Solution and Antibacterial Application

Gudisa Hailu Chala

A Thesis Submitted to the Department of Applied Chemistry,

School of Applied Natural Sciences

Presented in Partial Fulfillment of the Requirement for the Degree of Master of Science in Applied Chemistry (Inorganic Chemistry)

Office of Graduate Studies

Adama sciences and Technology University

November 2022

Adama, Ethiopia

Green Synthesis of Magnetite Nanoparticle Using *Catha Edulis* Plant Leaf Extract for Removal of Chromium from Aqueous Solution and Antibacterial Application

By: Gudisa Hailu Chala

Advisor: Dr. Tegene Dessalegn (Associate Professor)

A Thesis Submitted to the Department of Applied Chemistry
School of Applied Natural Science

Presented in Partial Fulfillment of the Requirement for the Degree of Master of Science in Applied Chemistry (Inorganic Chemistry)

Office of Graduate Studies

Adama sciences and Technology University

November 2022
Adama, Ethiopia

Declaration and Recommendation

Declaration

I hereby declare that this Master Thesis entitled "Green Synthesis of Magnetite Nanoparticle Using Khat (*Catha Edulis*) Plant Leaf Extract for Removal of Chromium from Aqueous Solution and Antibacterial Application" is my original work. That is, it has not been submitted for the award of any academic degree, diploma, or certificate in any other university. All sources of materials that are used for this thesis have been duly acknowledged through citation

Gudisa Hailu Chala _____ _____

Name of the Student Signature Date

Recommendation

I, the advisor of this thesis, hereby certify that I have read the revised version of the thesis entitled "Green Synthesis of Magnetite Nanoparticle Using Khat (*Catha Edulis*) Plant Leaf Extract for Removal of Chromium from Aqueous Solution and Antibacterial Application'' prepared under my guidance by **Gudisa Hailu Chala** submitted in partial fulfillment of the requirements for the degree of Mater of Science in Applied Chemistry (Specialization in Inorganic Chemistry). Therefore, I recommend the submission of the revised version of the thesis to the department following the applicable procedures.

Dr, Tegene Dessalegn	_____	_____
Advisor	Signature	Date

Approval Page

I, the advisor of the thesis entitled "Green Synthesis of Magnetite Nanoparticle Using Khat (*Catha Edulis*) Plant Leaf Extract for Removal of Chromium from Aqueous Solution and Antibacterial Application'' and developed by **Gudisa Hailu Chala**, hereby certify that the recommendation and suggestions made by the board of examiners are appropriately incorporated into the final version of the thesis.

Dr, Tegene Dessalegn _____ _____

Advisor Signature Date

We, the undersigned, members of the Board of Examiners of the thesis by **Gudisa Hailu Chala** have read and evaluated the thesis entitled "Green Synthesis of Magnetite Nanoparticle Using Khat (*Catha Edulis*) Plant Leaf Extract for Removal of Chromium from Aqueous Solution and Antibacterial Application" and examined the candidate during the open defense. This is, therefore, to certify that the thesis is accepted for partial fulfillment of the requirement of the degree of Master of Science in Applied Chemistry (Inorganic Chemistry).

Dr. Bedasa Abdisa _____ _____

Chairperson Signature Date

Dr. Gemechu Deressa _____ _____

Internal Examiner Signature Date

Dr. Endale Tsegaye _____ _____

External Examiner Signature Date

Final approval and acceptance of the thesis are contingent upon the submission of its final copy to the Office of Postgraduate Studies (OPGS) through the Department Graduate Council (DGC) and School Graduate Committee (SGC).

_____ _____ _____

Department Head Signature Date

_____ _____ _____

School Dean Signature Date

_____ _____ _____

Dean, Office of Postgraduate Studies Signature Date

ACKNOWLEDGEMENT

First let me start my thanks and glory to my almighty GOD, for providing me hope and strength.

I would like to express my gratitude to my advisor Dr, Tegene Dessalegn for his valuable advice, helpful discussions, devoted support, and guidance.

My heartfelt appreciation and honor also go to my father Hailu Chala and my Mother Dawiti Damesa for the material assistance and moral support.

I would like also to express my thanks to Dire Dawa University for moral support and sponsoring my education.

Finally, my thanks go to Adama Science and Technology University, Department of Applied chemistry, for various support and friendly assistance.

Table of Contents

LIST OF FIGURES

LIST OF ACRONYMS AND ABBREVIATIONS

DNA	Deoxyribose nucleic acid
DTA	Differential thermal analysis
EDX	Energy-dispersive X-ray examination
ELISA	Enzyme-linked immunosorbent assay
FTIR	Fourier Transform Infra-Red Spectroscope
FWHM	Full Width at Half Maximum
INP	Iron nanoparticles
IONP	Iron oxide nanoparticles
MIC	Minimum Inhibitor concentration
MHB	Muller Hinton broth
MNPs	Metal Nanoparticles
MW	Microwave
NPs	Nanoparticles
PFO	Pseudo first order
PSO	Pseudo second order
ROS	Reactive oxygen species
SEM	Scanning electron spectroscopy
TEM	Transmission electron microscopy
TGA	Thermogravimetric Analysis
UV-Vis	Ultra Violet Visible Spectroscopy
UV-Vis DRS	Ultra Violet Visiable Diffuse reflectance spectroscopy
XRD	X-ray diffraction
ZVI	Zerovalent iron

ABSTRACT

Hexavalent Chromium pollution in aquatic environments is a serious problem for living organisms and public health. In addition, the emergence of drug resistant bacterial strains has become a threat to human health. A number of researches are being carried out to address the problem and minimize chromium related pollutions and also search for alternative metal based antibacterial treatments. In this study Magnetite (Fe_3O_4) Nanoparticles synthesized using Catha edulis plant leaf extract were investigated as adsorbent for Cr(VI) removal from aqueous solutions and also as antibacterial agent. The synthesized NPs were characterized by using X-ray diffraction (XRD) spectroscopy, Fourier Transforms Infrared (FTIR) spectroscopy, Scanning Electron Microscopy (SEM), Ultraviolet-visible (UV-Vis) spectroscopy, and thermal analysis (TGA-DTA). The XRD result revealed that the phase structure of Fe_3O_4 NPs was cubic face-centered with crystallite sizes of 12.1 nm, 14 nm, and 9 nm for metal to plant extract ratios of 1:1, 2:1, and 1:2 NPs respectively. UV-vis DRS confirmed band gap energy of synthesized NPs was found to be ranging from 2-2.5 eV. The batch adsorption experiment was used to evaluate the efficiency of the adsorbent by varying the different parameters such as pH (3-10), adsorbent dose (250mg – 1250mg), initial concentration of adsorbate (20mg/L - 60mg/L), and contact time (20-100 min) at room temperature. The concentrations of Cr(VI) were measured using ultraviolet-visible (UV-Vis) spectrophotometry with 1, 5 diphenylcarbazide at 540 nm. Cr(VI) removal efficiency of Fe_3O_4 was found to be 98.6% from an aqueous solution at the initial concentration of 20 mg/L. The experimental data were best fitted to the Freundlich adsorption isotherm model (R^2 = 0.98341). Moreover, the mechanism of adsorption was in good agreement with pseudo 2nd order kinetics (R^2=0.98188). The results suggested that the biosynthesized Fe_3O_4 nanoparticles have the potential for the removal of hexavalent chromium ions. In addition to this, the synthesized Magnetite (Fe_3O_4) Nanoparticles were evaluated for antibacterial activity by the disk diffusion method and 100µg/mL concentrations of Fe_3O_4 NPs (1:2) showed better activity against S. aureus with a zone of inhibition of 12 mm followed by S. pyogen and E.coli with zone of inhibition of 11 mm in both cases.

Keywords: Green synthesis, Magnetite NPs, *Catha edulis*, Adsorption, Antibacterial activity

1. INTRODUCTION

1 .1 Background of the Study

Heavy metal ions in aquatic environments are serious pollution problems for living organisms and public health. Heavy metals are non-biodegradable and tend to bioaccumulate. Hexavalent chromium ion is a common industrial pollutant posing serious ecosystem threats. Strong Cr^{6+} oxidizing properties cause toxic effects on biological systems. Chromium is commonly released to the environment from leather tanning, metal processing, electroplating, pigment synthesis, dying, wood protection, electrical and electronic equipment, (Rajput et al., 2016).

Inhalation and retention of chromium (VI) containing material can cause developmental issues, damage to the skin, respiratory, reproductive, and digestive systems, and cancer. Cr (VI) is much more toxic than Cr(III) because of its greater ability to enter cells and its strong oxidation potential. Once inside cells, Cr(VI) is reduced and produces free radicals, Cr(V), Cr(IV), and eventually Cr(III), which are believed to be responsible for toxic and carcinogenic effects (Dhal et al., 2018). Therefore, it is essential to regulate the concentration of heavy metals in wastewaters before their disposal in the environment (Weijiang et al., 2017).

There exist a number of methods of removing heavy metals from aqueous system. However, due to various reasons, there are challenges with the efficient removal of heavy metals from wastewater before being discharged into the environment. So far several pioneering strategies have been developed to address the aforementioned challenges. Chemical precipitation, ion exchange, adsorption, ultrafiltration, constructed wetland, and membrane separation have been used for metal removal (Rajput et al., 2016).

Adsorption is the most commonly used technique for the removal of chromium from wastewater due to it is high removal efficiency, regeneration of adsorbent, low cost, easy operation, and absence of secondary pollutant formation (Jadidi et al., 2017)

Among the commonly used adsorbents, bio-synthesized nanoparticles are the most prominent candidates because they are reproducible, non-toxic, environment-friendly, and low-cost adsorbents with relatively high adsorption capacity (Michael et al., 2020)

Recently, several researchers have reported synthesis of nanoparticles via a green chemistry approach, which can be used as an effective adsorbent for heavy metals. However, there are few or no reports of research related to the green synthesis of magnetite nanoparticles using *Catha edulis* Plant leaf extract as capping and /or reducing agent. And it is applications in wastewater treatment are rarely reported.

The emerging bacterial resistance to the current drugs is also another challenge that needs intervention. Human pathogenic bacteria have developed resistance to most of the antibiotics in the market. This necessitates the urgency to find potent antimicrobial agents, especially from biosynthesized nanoparticles (Microbes, 2016).

In the current study, *khat* (*Catha edulis*) leaf extract was used as a reducing and capping agent for the synthesis of magnetite nanoparticles. *Khat* (*Catha edulis*) leaf extract contains phytochemicals such as alkaloids, cathine and dimer of cathinone, triterpenes, sterols, fatty alcohols, hydrocarbon carboxylic acid, and saponins. The alkaloids, cathinone, are presumably the main psychoactive component of *Khat* (Kiflom Gebremedhn et al., 2019). Additionally, the leaf extract was chosen, since they're environmentally available and contain chemical constituents that would act as reducing and capping agents. Studies have indicated that biomolecules like polyphenols, saponins, organic acids, vitamins, polysaccharides, and terpenoids play a task in reducing and capping nanoparticles. Currently, there's an increasing demand to develop environmental friendly nanoparticle synthetic processes that are free from toxic chemicals within the synthesis protocol. As a result, researchers within the field of nanoparticles synthesis and assembly have turned to the biological system (Bolade et al., 2020)

Green synthesized magnetite nanoparticles were chosen as nano adsorbents exhibit higher efficiency and faster adsorption rate due to it is small size, high porosity, large active surface area, high reactivity, catalytic efficiency, and it's superparamagnetic properties and also showed better antimicrobial properties, because of Fe_3O_4 NPs have Small size, large surface area and a high degree of dispersion of NPs make them unique in terms of catalytic activity and can also contribute to their penetration through bacterial membranes, thus leading to bactericidal effects (Asab et al., 2020)

The nanoparticle surface and chemical properties were characterized and they were confirmed as promising adsorbents for aqueous hexavalent chromium ion elimination. Solution pH, contact time, adsorbent dose, and initial metal concentration were investigated and kinetics, equilibrium adsorption parameters, and reusability were evaluated. The adsorption behavior and mechanism were investigated. And also magnetite nanoparticle antibacterial activities were investigated against gram-positive and gram-negative bacteria strains.

1.2 Statement of the Problem

These days, the increasing prevalence of heavy metal pollution in aquatic environment and emerging bacterial drug resistance to existing antibiotics are among the major human health concerns. To address these issues, researchers are striving their best to come up with efficient and potential alternative solutions. The green synthesis of nanoparticle using plant extracts for removal of hexavalent chromium from waste water and antimicrobial activity application study are thoroughly investigated. This study has tried to investigate the efficiency green synthesized magnetite NPs for removal of Chromium from aqueous solution and antibacterial activity of the NP against selected gram positive and gram-negative bacterial strains. There are many physical, chemical, and biological purification methods available to get rid of heavy metal pollutants from wastewater.

The undertaken study adopted adsorption technique which is the most commonly used physical technique, efficient to get rid of inorganic and heavy metal pollutants from waste water. There exist different adsorbents that have been used to remove chromium from wastewater. The search for adsorbents with high removal capacity, low cost and easy accessibility as a choice for industrial wastewater treatment process has motivated our group to do the current study.

The second problem is the recent emergence of antibiotic resistance and related toxicity issues that limit the use of currently available antimicrobial agents. Therefore investigation of the potential antibacterial agents specially using NPs remains topic of research interest

Therefore, in this research it was intended to use magnetite nanoparticles which were synthesized by employing green method using khat (*Catha edulis*) leaf extract as nano adsorbents for hexavalent chromium removal and as potential antibacterial agent.

1.3 Objective of the Study

1.3.1 General objective of the Study

The overall objective of this study was to synthesize and characterize magnetic magnetite nanoparticles using khat (*Catha edulis*) for the removal of hexavalent chromium from waste water and to evaluate the antibacterial effect of the NPs

1.3.2 Specific Objective of the Study

i. To synthesize and characterize magnetite nanoparticles using khat (*Catha edulis*) plant leaf extract,
ii. To study the removal of chromium from waste water using the synthesized nanoparticles
iii. To evaluate the effect of pH, contact time, adsorbent dosage, and initial concentration of metal ion on the adsorption efficiency of the nanoparticles
iv. To determine the chromium adsorption mechanism on green synthesized magnetite nanoparticle
v. To investigate the antibacterial activities of magnetite nanoparticles by using the disc diffusion method against gram-positive and gram-negative bacteria strains

1.4 Significance of the Study

The greatest advantage of this study is that the magnetite nanoparticle was synthesized by a green process from *Catha edulis* extraction the method which is ecofriendly and the produced adsorbent could be an alternative in waste water treatment approaches, Generally, this study provided information regarding the application of magnetite nanoparticles for hexavalent chromium removal from wastewater by adsorption process and its antibacterial activity. Moreover, the findings of this study would be used as a baseline by other researchers for further study in the area.

1.5 Scope of the Study

This research work was limited to green synthesis magnetite (Fe_3O_4) nanoparticle using khat (*Catha edulis*) plant leaf extract and characterization of the nanoparticle using XRD, FTIR, SEM, TGA, and UV-Vis DRS techniques and evaluation of the efficiency of the NPs for removal of hexavalent chromium from waste water, and antibacterial activity.

2. LITERATURE REVIEW

2.1 Nanoparticles

Nanoparticles are particles within the nanoscale size between 1-100nm with a surrounding interfacial layer. The green synthesis route of nanoparticles has received tons of attention from researchers to clarify the mechanism of synthesis. Almost every sort of biological entity has been used to synthesize nanoparticles in a regulated manner by size and shape. Green synthesized metal nanoparticles are studied by researchers due to their unique characteristics, and therefore the biomolecules contained within the plant extract play a crucial role as both stabilizing and reducing agents (Kumavat & Mishra, 2021).

Researchers are trying to synthesize nanoparticles with new properties to increase the range of their applications. Improving wastewater management using nanoparticles is one of the major focuses of nanotechnology. An overview of - new advances happening in this area of research is discussed subsequently. Some of the major nanotechnology methods used for water treatments are nano adsorption, membrane filters with nanoparticles, photocatalysis, and antimicrobial or disinfectant treatment using nanoparticles. Nanotechnology is emerging as a promising technology, which has demonstrated remarkable feats in various fields including wastewater treatment. Nanomaterials encompass a high surface-to-volume ratio, high sensitivity and reactivity, a high adsorption capacity, and ease of functionalization which makes them suitable for application in wastewater treatment (Jain et al., 2021).

Investigations showed that the NPs size is the significant parameter that determined the antimicrobial effects of those materials. Bacterial cell walls attract NPs to their surface due to electrostatic interactions. These NPs establish a robust bond with membranes, leading to increased cell wall permeability. Metal NPs and metal ions, released from NPs, are capable of entering the cell and disrupting cell functions by inducing oxidative stress and suppressing the antioxidant defense reaction of bacteria against reactive oxygen species. Then, these ions are liberal to interact with cellular structures and form strong and non-specific coordination bonds with N, O, or S atoms of organic compounds which end up disrupting biological processes in a wide selection of microorganisms (Sallak et al., 2021.)

2.2 Metal oxide Nanoparticles

Metallic oxide nanoparticles are nano-sized (width, thickness, length) in the range of 1 –100 nm. Metal oxide nanoparticles are attractive for a large variety of applications including catalysis, sensors, electronic materials, and environmental remediation. Controlled synthesis of metal oxide nanoparticles is necessary for a successful application, and solution-phase methods provide a large degree of control over the synthesis products (Article, 2006).

2.3 Iron oxides Nanoparticles

Among the nanoparticles synthesized, iron-based nanoparticles have considerable importance due to their, magnetic property, catalytic activity for removal of pollutants from water bodies, their cheap cost, (The second most abundant element on earth), high reactivity, selectivity, surface area, high grade of functionalization, high adsorption capacity for several contaminants in water and wastewater treatment and its notable antimicrobial and antioxidant activity (Aragaw et al., 2021).

Iron oxides is a combined term for oxides, hydroxides and oxy-hydroxides made up of Fe (II) and/or Fe (III) cations and O^{2-} and /or OH^- anions. Currently, sixteen pure phases of iron oxide are acknowledged. These are Fe $(OH)_3$, Fe $(OH)_2$, Fe_5HO_8-$4H_2O$, Fe_3O_4, FeO, five polymorphs of FeOOH, and four of Fe_2O_3. Magnetite (Fe_3O_4), and hematite are the most known oxide forms of Iron. Research on the ZVI oxidation or aging has so far acknowledged several products, including goethite, akaganeite, lepidocrocite, magnetite), maghemite, green rusts I/II (a group of bluish-green Fe(II)–Fe (III) hydroxyl salts), siderite ($FeCO_3$), and iron sulfide, etc. In addition to the above oxyhydroxides forms feroxyhyte, ferrihydrite, better recast as FeOOH-$0.4H_2O$, and high-pressure FeOOH is another oxide/hydroxide form of iron oxides. Iron oxide nano adsorbents such as hematite, maghemite, and magnetite (Fe_3O_4) have been widely utilized by researchers for the removal of various pollutants such as As(V), Cr(VI), $Cr_2O_7^{2-}$, MnO4, Cu(II), Pb(II), and Hg(II) from environmental or industrial effluents (Assefa & Mazengiaw, 2021).

2.3.1 Magnetite (Fe_3O_4) Nanoparticles

Magnetite is a common magnetic iron oxide that possess a cubic inverse spinal structure with oxygen forming an 'fcc' closed packing and Fe cations occupying tetrahedral sites and octahedral sites. Magnetite nanoparticles have a large area of application in fields such as magnetic separation, storage, biomedical applications, chemical industries and water purification (Rahman et al., 2013)

The structure of magnetite nanoparticle gives it special properties so that it is often utilized in many medical, pharmaceutical, and therapeutic applications (Hajba & Guttman, 2016). Magnetite nanoparticle is a much known nano-adsorbent. Its foremost physiochemical properties, cheap strategy, and straightforward recovery within the sight of out of doors attractive fields make it a commonly prepared material for water treatment (Aragaw et al., 2021).

Silica Supported Iron Oxide Nanoparticles was synthesized and used for removal of Cr(VI) from aqueous solutions by the adsorbent iron oxide NPs-SiO_2 at room temperature showed a strong dependency on the pH of the solution, adsorbent dosage, initial Cr(VI) concentration, and contact time, their overall results showed the synthesized nanoparticle effectively remove Cr(VI) from aqueous solutions (Edris et al., 2019).

Magnetic nanoparticles also offer several advantages for various applications including biomedical like that antimicrobial. Moreover, they are essential in the protection of environmental pollution (Sathya et al., 2018). The adsorptive and reductive capabilities of iron-based nanoparticles have made them considerable environmental remediation agents, particularly in situ processes. They are cheap, non-toxic, and effective for the degradation of a wide range of contaminants organic and inorganic (Bolade et al., 2019).

2.4 Synthesis of Nanoparticles

Stabilized noble metals NPs have been produced by the use of numerous techniques. These techniques are generally categorized into the bottom-up and top-down processes. In the bottom-up method, nanosize assemblies have been formed via way of means of molecular components. Whereas, within side the top-down method, nanoparticles are generated from their constituent metals with the helped of the reserved microscopic device and transformed

into nanoscale dimensions (Armbrüster & Cardoso-Gil, 2015). There are three main routes for the synthesis of Fe_3O_4: chemical, physical and biological. These have been investigated to produce more stable, soluble, biocompatible, and shape and size-controlled nanoparticles (W. Wu et al., 2008)

2.4.1. Physical Method

Physical technique for synthesizing NPs is mainly a "top-down" technique where in which material is reduced in size by various physical approaches like ultra-sonication, microwave (MW) irradiation, electrochemical technique, etc. In this technique, a tube heater is applied at barometrical weight for integrating NPs by evaporation condensation. Evaporation Condensation and laser elimination are the maximum important physical methodologies. The source material inside a pontoon targeted on the heater is vaporized right into a bearer gas. The advantage of these strategies are speed, radiation used as lowering agents, and no dangerous chemical substances involved, however, the downsides are low yield and excessive power consumption, solvent contamination, and absence of uniform distribution (Zhang et al., 2016).

2.4.2. Chemical Method

Chemical preparation methods are simple, tractable, and efficient, in which the size, composition, and even the shape of the NPs can be managed. Fe_3O_4 can be synthesized through the co-precipitation of Fe^{2+} and Fe^{3+} by the addition of a base. The size, shape, and composition of Fe_3O_4 NPs synthesized through chemical methods depend on the type of salt used, Fe^{2+} and Fe^{3+} ratio, pH, and ionic strength (S. Wu et al., 2011). The benefit of the chemical synthesis of nanoparticles are the easy production, low cost, and excessive yield; however, the usage of chemical reducing agent is dangerous to live organisms (Zhang et al., 2016)

2.4.3 Biological Method

Biological syntheses of nanoparticles are extra convenient, cost-effective, and environmentally-pleasant manner than the chemical or physical method. By using the green method, huge-scale manufacturing of nanoparticles is constantly a difficult mission and those are operated best in a laboratory-scale manner. However, huge-scale production is possible in near future without using any powerful machines and advances in studying the nature of

biological extracts composition along with the reaction with metal ions (Sathya et al., 2018).

2.4.3.1 Green synthesis using Microbes

Microorganism-based synthesis of nanoparticles has gained attention within the past few decades thanks to its benefits over conventional chemical syntheses. These advantages include synthesis at temperature an energy-efficient process, consumption/ production of less toxic chemicals/ by-products, natural abundance, simple proportion, and ability to cope in extreme conditions. Microorganisms like fungi, bacteria, and yeast can synthesize nanoparticles via the extracellular or intracellular mechanism. These processes entail the enzymatic reduction of metal ions, producing well-dispersed nanoparticles with a small size distribution, with proteins, peptides, and genes acting as natural capping agents, which successively provide stability and reduce agglomeration of nanoparticles. Unlike in extracellular mechanism, which involves enzymatic reduction of metal ions sure to the cell wall/surface of microorganism electrostatically, the metal ions diffuse into the cell where they react with enzymes to make nanoparticles in intracellular mechanism (Bolade et al., 2020)

Magnetic iron oxide nanoparticles of 32–48nm average particle size was synthesized using cultured strains of Micro bacterium marinilacus isolated from sediment samples collected from Damodar River in India. 1mM of the precursor solution (ferric chloride solution) was added to the isolated bacterium and incubated leading to the formation of nanoparticles marked by a color change of the culture from brown to dark brown within 2h. To separate the synthesized nanoparticles from cells, the culture was centrifuged, the supernatant was separated, dehydrated, and characterized using scanning microscopy (Mukherjee et al., 2017).

2.4.3.2 Green synthesis using Biomolecules

Simple and versatile method of enzyme catalysis and nanoparticle synthesis using a common platform, poly (acrylic acid)-coated polyvinylidene fluoride membrane, and “greener” methods was developed. The enzymes were incorporated in polymer multilayer-assembled membranes through electrostatic interactions and maintained a high activity upon immobilization comparable to that of the homogeneous phase catalysis. Membranes

containing different enzymes can be stacked and used as reactors in series and the reaction yields can be modulated by adjusting parameters such as the enzyme loading on each membrane and the residence time, which is in turn related to permeate flux. We have demonstrated the direct and "green" synthesis of bimetallic Fe/Pd particles in a membrane domain. Compared to the established method, which uses toxic sodium borohydride, this approach uses biodegradable ascorbic acid and thus has a minimized environmental impact (Smuleac et al., 2011).

2.4.3.3 Green synthesis using Plants and Phytochemicals

The process of synthesizing zerovalent iron nanoparticles using plant materials such as leaves, stems or backer lies upon the successful extraction of bioactive components of the plant materials. These compounds include polyphenols, saponins, organic acids, vitamins, and polysaccharides, which are soluble in water, and some organic solvents such as methanol and acetone. Subsequently, they act as capping and reducing agents when reacted with a precursor mostly iron (III) chloride solution. The reduction of Fe^{3+} to Fe^{0} results in the formation of zero-valent ion nanoparticles (Bolade et al., 2020).

Synthesized zero-valent iron using polyphenols obtained from dried green tea extract. Polyphenols, which are abundant bioactive compounds especially in leaves of several plants, were microwave-extracted from green tea leaves to obtain nanoparticles with particle sizes ranging from 8 to 23 nm. Powdered green tea leaves were extracted with ethanol, allowed to cool, and then filtered. Plant extract containing polyphenols was reacted with iron (III) chloride solution to synthesize Zerovalent iron nanoparticles (Borja et al., 2015).

2.5 Khat (*Catha edulis)* Plant

Khat (*Catha edulis*) belongs to the *Celastraceae* family which contains 60–70 genera and 850–900 species. Khat is most commonly grown in the horn of Africa and southwestern Arabia. *Khat (Catha edulis)* has been recognized as an addictive drug. The substance causes physical addiction and has a side effect that is commonly related to increasing medical complications. I argue that there is a need to develop khat (*Catha edulis*) based nanoparticles for wastewater treatment and antimicrobial activity rather we use them as addictive drugs. Khat contains several phytochemicals such as alkaloids (phenylalkylamines and *Catha edulis*), flavonoids, steroid and triterpenoids, monoterpenes, volatile aromatic compounds, and other

miscellaneous compounds like vitamins and amino acids which are used as reducing and capping agent for the synthesis of magnetite nanoparticle (Getasetegn, 2016).

2.6 Applications of Magnetic Nanoparticles

The synthesis of magnetic nanoparticles (MNP) has received great interest in recent years because of the new physical and chemical properties of materials at the nanoscale. These properties make them suitable for applications in various fields like medicine, chemistry, environment, energy, agriculture, information, and communication, heavy industry, and commodity. The iron and iron-based nanoparticles have a good range of applications like biomedical, environmental, textiles, health care, food industry, electronics, renewable energy, etc. The removal of metal and dye from wastewater and spring water using adsorption study and antimicrobial activity is one among the preliminary applications (Sathya et al., 2018).

2.6.1 Wastewater treatment

Wastewater contains several dangerous and harmful materials and it originates from various sources, which incorporates sewage, industrial waste, commercial waste, and agricultural waste, which might be characterized by their physical appearance, chemical composition, and a lot of microorganisms. Generally, wastewater comes from normal living processes, or in other terms wastewater is any water that has been contaminated by human use, the main sources of wastewater are domestic wastewater, agricultural waste, industrial waste, and commercial waste (Jain et al., 2021). Water contaminants can be geological or anthropogenic or man-made. Higher levels of contaminants in drinking water seldom cause acute health effects. The naturally occurring elements present at unacceptable levels can contaminate water (Jain et al., 2021).

If we consider the most source of water, we can observe different sources of pollution, metal processing, beverages, textiles, chemicals, floriculture, paints, paper, pesticide, cement, plastic, and tanneries wastes. Exposure to these wastes which contain toxic components such as trace metal ions, is of great concern, as it poses not only health risks to humans but also potentially unacceptable ecological risks to plants that are produced by intensive agricultural practices along with the riversides, animals, and microorganisms (Gebeyehu et al., 2020). Communities depend on our streams and rivers to deliver much of these water uses. Without adequate quantity and quality of freshwater sustainable development will not be true for all

countries around our globe. In Ethiopia from the increasing human population, uncontrolled urbanization and waste disposal cause serious quality degradation of surface waters. Now a day's water pollution from the disposal of industrial wastewater is becoming an environmental concern in Ethiopia (Mulu et al., 2015).

2.6.2 Biological applications for iron oxide Nanoparticles

Metal and metal oxide nanoparticles possess unique structure, high surface area, biocompatibility, interesting redox and catalytic properties, and good mechanical stability. Due to these properties and unique plasmonic properties, metal and metal oxide nanoparticles have considerable attention in the field of biomedical applications like bio imaging, biomedical therapeutics, bio sensing, implant devices, neurochemical monitoring and diagnostics (Ali & Ahmed et al., 2018). Iron oxide is the material that is investigated the most in biomedical techniques, due to its superior biocompatibility with respect to other magnetic materials, both based on oxides or on pure metals.

2.6.2.1 Antimicrobial Activity

Drug and antibiotic resistance is a growing issue, necessitating the creation of new, more potent medications to combat bacteria. The horizontal gene transfer of the antibiotic resistance genes, modification of the antibiotic target, mutational alterations in the formation of biofilms, and efflux pumps are all causes of resistance in bacteria. The fear of multidrug resistant parasites and diseases emerging and reappearing is a result of patterns of antibiotic resistance in microorganisms. Therefore, modification in antimicrobial compounds to augment their latent bactericidal prospective is a main area of research in modern era and nanotechnology provides an excellent platform to transform and develop the important properties of metal in the form of nanoparticles having potential applications as cell labellers, biomarkers, contrast agents for bio imaging, antimicrobial agents, and drug delivery schemes (R. Singh & Nalwa et al., 2011). The unique physicochemical characteristics of nanomaterials have positioned them to exercise multiple actions against multidrug resistant bacteria for broader applications. It was predicted that the particles rendered the drug-resistant isolates vulnerable by a series of attacks; comprising deformation of structural integrity of bacterial cell wall to stimulate entry of particles, in addition to the enhancement of the entry of antibiotic via the carrier action of the particles. Studies suggest that the potential of magnetic IONPs nanoparticles to generate

microbial toxicity is due to a series of interactions, including membrane depolarization with consequent impairment of cell integrity, production of reactive oxygen species (ROS) with lipid peroxidation and DNA damage, and release of metal ions that affect cellular homeostasis and protein coordination (Pessan et al., 2018).

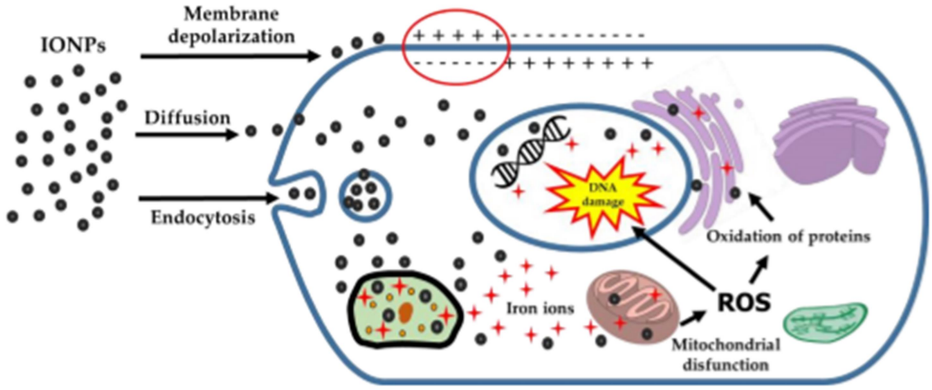

Figure 1 mechanism by which iron oxide nanoparticles (IONPs) generate cell toxicity and reactive oxygen species.

2.6.2.2 Bio imaging Application

MRI has been developed into one of the most powerful imaging tools in clinical radiology. However, the sensitivity at cellular/molecular level is obviously lower than positron emission tomography and fluorescence imaging. To obtain contrast enhancement and signal amplification, magnetic iron oxide nanoparticles have been widely used in clinical settings for many years (Liu et al., 2013)**.** Iron oxide NPs are studied as a passive and active targeting imaging agent because they are superparamagnetic. They have iron oxide core with a hydrophilic coat of dextran or other biocompatible compound to increase their stability. They are mostly used in MRI. Till now, two SPIO agents, ferumoxides (120-180 nm) and ferucarbotran (60 nm) are clinically approved for MRI (Anwar et al., 2018).

2.6.2.3 Drug delivery

Most of the chemotherapeutics agents distribute to the whole body results in toxicity and it gives poor compliance by patients, so as targeted delivery of therapeutic agents to tumour cells is a challenge. By active and passive targeting, imaging of tumour cells is done by metallic

nanoparticles. Both at surface and inside cells, metallic nanoparticles can interact with bio molecules because of their small size which gives better targeting for therapeutics (Nanoliposomes, 2013) . Between 10-100nm of different shapes, sizes of gold, nickel, silver, iron metallic nanoparticles have been checked out as diagnostics and drug delivery systems. Magnetic nanoparticles have greater reactive area and ability to cross biological barriers than their micrometric counterparts, which favors their use in drug delivery systems. In this context, different classes of drugs can be directly bound to IONPs or to core-shell nanosystems. Such binding can occur by adsorption, dispersion in the polymer matrix, encapsulation in the nucleus, electrostatic interactions and covalent attachment to the surface, aiming to improve their pharmacological properties. IONPs have been used as carriers of anticancer, alternative, immunosuppressive, anticonvulsant, anti-inflammatory, antibiotic and antifungal agents (Pessan et al., 2018)

2.7 Removal Methods of Water Contaminants

Nanotechnology-based pathways, which are being employed for wastewater remediation, are adsorption and biosorption, nanofiltration, photocatalysis, disinfection, pathological control, sensing, monitoring, and so on (Rajput et al., 2016).

2.7.1 Adsorption

Adsorption is reckoned as the accrual of mass between two phases on the surface or at the interface. The material that accumulates over the surface is known as adsorbate and the surface on which accrual occurs is called adsorbent. It is categorized into physical and chemical adsorption. In chemical adsorption (or chemisorption), there is an ionic or chemical interaction between adsorbent and adsorbate. Generally, chemical adsorption is an irreversible process and is found to be highly efficient. In physical adsorption, the accumulation of mass is because of weak attractive Vander Waals forces, hydrogen bonding, polar-polar interaction, etc., and the process is reversible in most cases. Apart from the removal of dyes adsorption, using the chemical adsorption approach is widely used for removing heavy, toxic, or precious metals, anionic groups, toxic organic compounds, and pollutants (El-Sheikh et al., 2018). Other techniques are usually not attractive due to their high operation costs and the time-consuming processes involved. Adsorption, however, has proved to be a more powerful

technique for treating inorganic pollutants as it is inexpensive, easy to perform, and insensitive to toxic substances (Sheshmani & Mashhadi, 2018).

2.7.2 Magnetite (Fe_3O_4) Nanoparticles for removal of Chromium from Waste Water

The interest in Magnetite Nanoparticles for heavy metal ions removal has been increasing due to their enhanced reactivity as a result of very high surface area to volume ratio. Cr (VI) has been accounted to be responsible for lung disease, chrome ulcer, aperture of the septum, and mind and kidney harm. The important reason for its intense danger is its fast diffusivity through the skin which empowers it to reply with natural frameworks and harm sundry organs Fe_3O_4 nanoparticles showed great adsorption ability for deliberation of Cr(VI) (Namdeo, 2018) .Magnetite Nanoparticles have been shown to be an effective adsorbent for adsorption of Cr(VI). Electrostatic attraction forces between Cr(VI) ions and magnetite NPs play a key role for the Cr(VI) removal. The adsorption process was found to be strongly dependent on pH, contact time, adsorbent dose, and initial Cr(VI) concentration. Additionally, the magnetic separation of Fe_3O_4 NPs from solution is more rapid, simpler, and more effective than other solid–liquid separation techniques (Çiftçi et al., 2017).

2.8 parameter that affects the Removal of chromium (VI) by adsorption

2.8.1 Effects of solution pH

Removal efficiency increase with increasing solution pH until equilibrium is reached. This is often the very fact that increasing pH results in the formation of charge on the surface of adsorbent abreast of deprotonation reaction. This charge enables high removal efficiency as a result of electrostatic attraction between the adsorbent and charged adsorbate, whereas at lower pH, the varied functional groups and reactive atom of adsorbent protonated, and both get charged. The maximum removal efficiency of hexavalent chromium is higher at low pH, as the pH was increased from 3 to 10 efficiency decreased. The optimum pH was 3.0 and all other experiments were done at this pH. As pH increases, the surface of magnetite nanoparticles becomes more negatively charged. This causes increased repulsion between Cr (VI) and magnetite nanoparticles (Padmavathy et al., 2016)

2.8.2 Effects of adsorbent dose

As adsorbent dosage increases keeping all the other parameters at constant value removal efficiency first increases, reaches the maximum, and then decreases. As adsorbent dosage increases chromium uptake decreases. At lower adsorbent concentrations number of active sites is higher. With the increase in adsorbent dosage aggregation of particles takes place, as a result, efficiency and Cr uptake decrease (Padmavathy et al., 2016). If adsorption dosage is decreased, the quantity of adsorbed material is decreased, due to the aggregation and overlapping of particles of adsorbent within the solution, consequently, a decrease within the surface for heavy metal uptake occurs (Abate et al., 2020)

2.8.3 Effects of initial concentration of Chromium

The initial concentration of the contaminant is important in adsorption since a given mass of sorbent material can only absorb a fixed amount of ions. Normally, the removal capacity of the adsorbent will decrease with an increase in initial contaminant concentration. This is because for a given mass of adsorbent material; the amount of ions that can be adsorbed is fixed. The C r(VI) uptake was quite fast toward the beginning, followed by a much slower subsequent removal and at last leading to a steady state (Yuan et al., 2010).

2.8.4 Effect of contact time

To see the rate and effectiveness of any wastewater treatment process, it is very important to study the effect of time. The time of contact between the adsorbate and adsorbent is the determinant factor of the kinetics and equilibrium of the adsorption process. (Chen et al., 2011) reported the concentration of metal ions adsorbed from wastewater increases with the prolonged time. The uptake of heavy toxic metals is examined at different time intervals (0-250). The results indicate that the adsorption equilibrium is reached after only 50 min.

2.9 Adsorption isotherm Studies

Adsorption isotherms describe how the adsorbate interacts with the adsorbent and supply a comprehensive understanding of the character of the interaction. Isotherms help to supply information about the optimum use of adsorbents. Isotherm curves are extremely relevant for adsorption purposes since it provides information about the interaction mechanisms and maximum adsorption capacity of a determined adsorbent (Abate et al., 2020).

2.9.1 Langmuir isotherm Model

The basic assumption is that the sorption takes place at specific homogeneous sites within the adsorbent (Abate et al., 2020). These are comparably improved models of isotherm in explaining the adsorption of chemicals. The Langmuir isotherm is given by the following equation:

$$\frac{Ce}{qe} = \frac{1}{bqm} + \frac{\mathrm{Ce}}{qm} \qquad \text{……. (1)}$$

where Ce is the equilibrium concentration of solute (mmol L^{-1}), q_e is the amount of solute adsorbed per unit weight of adsorbent (mmol g^{-1} of adsorbate), q_m is the adsorption capacity (mmol g^{-1}), or monolayer capacity, and b is a constant (L $mmol^{-1}$) for Langmuir isotherm. The isotherm curves were drawn Ce/qe versus Ce for Langmuir isotherm (Abate et al., 2020).

2.9.2 Freundlich isotherm Model

The Freundlich isotherm is derived by assuming a heterogeneous surface with a non-uniform distribution of heat of adsorption over the surface. The mathematical expression for the Freundlich isotherm model is:

$$log\ Qe = log\ kf + \frac{\log \mathrm{Ce}}{n} \qquad \text{……. (2)}$$

where Ce is the equilibrium concentration of solute (mmol L^{-1}), q_e is the amount of solute adsorbed per unit weight of adsorbent (mmol g^{-1} of adsorbate), K_f and n are empirical constants for Freundlich isotherm incorporating all parameters affecting the adsorption process such as sorption capacity and sorption intensity respectively. The isotherm curves were drawn log q_e vs log c_e graph for the Freundlich isotherm model (Beyan et al., 2022).

2.10 Adsorption kinetics study

To determine the rate-limiting step during the adsorption process different kinetic models have been used to analyze the experimental data. These models include first-order and pseudo-second-order.

2.10.1 Pseudo-First order Model

The pseudo-first-order (PSO) kinetic model explains the relationship between the rate at the sorption sites of the adsorbents occupied and the number of unoccupied sites. It is defined using the Lagergren's equation as follows (Moussout et al., 2018):

$\frac{dqt}{dt} = k_1 (q_e - q_t)$……. (3)

where, q_e and q_t are the amounts of adsorbate uptake per mass of adsorbent at equilibrium and at any time with respect and K (min^{-1}) is the rate constant of the PFO equation. Integrating equation (3) for boundary conditions (t=0, $q_t = 0$, and t = t $q_e = q_t$) lead the following equation:

$\ln (q_e - q_t) = \ln q_e - k_1 t$ …….(4)

This can be rearranged in a nonlinearized form

$q_t = qe\ (1 - e^{-k_1 . t})$ ……..(5)

2.10.2 Pseudo-second order Modeling

The pseudo-second-order model is based on the adsorption capacity of the solid phase, and it visualizes chemisorption as the rate-controlling step. The pseudo-second-order kinetic is expressed in linear form in the following equation:

$\frac{1}{qt} = \frac{1}{k2\ qe^2} + \frac{1}{qe * t}$…… (6)

where qe (mg/g) is the amount adsorbed at equilibrium time; qt (mg/g) is the amount adsorbed at a time, t (min); k_2 is the pseudo-second-order rate constant; k diff (mg/g min1/2) is the interparticle diffusion rate constant, and C is the intercept that indicates the boundary layer thickness. The kinetic rate constant, k, and qe for each model can be calculated by plotting graph log t/qt versus t for pseudo-second-order models (Pitchay et al., 2022)

2.11 Antibacterial activity of Metal oxide Nanoparticles

Physiochemical and morphological properties of metal oxide nanoparticles have been demonstrated to exert an effect on their antimicrobial properties. Small nanoparticles monitor the strongest bactericidal effect, the positively-charged surfaces of metals and metal oxide nanoparticles facilitate their binding with the negatively-charged surfaces of bacterial cells,

which may result in the augmentation of the bactericidal effect. The shapes of nanoparticles also affect their antimicrobial activity (Wahid et al., 2017)

2.11.1 Antibacterial activity of Magnetite Nanoparticle

Iron oxide have a potential candidate for antibacterial application because of it is small size, unique superparamagnetic properties, and low toxicity make them a highly promising material for antibacterial application (Taimoory et al., 2018). For instance (Sathishkumar et al., 2018) synthesized Fe_3O_4 nanoparticles using the aqueous fruit extract of edible *C. guianensis.* The synthesized magnetite nanoparticle possesses a stupendous bactericidal effect against different bacterial human pathogens.

2.11.2 Method for Antibacterial activity test

The most common method used to evaluate the antibacterial effects, inhibition zone diameter of four multidrug-resistant pathogens, *S. aureus and S. pyogen* (gram-negative bacteria) and *E. coli and P. aeruginosa* (gram-positive bacteria) is the agar well diffusion method. The agar well diffusion method consists of making wells of 6 mm in diameter by punching an agar plate with a glass tube under sterilized conditions. Aliquots of 50 μL of each IL were placed on the wells, using physiological water for the control wells. The agar plates were incubated at 37 °C for 18-24 h and then, the radius of the inhibition zone around the wells was determined (Sepasgozar et al., 2022). First, for the bacterial strain, the cell suspension with 0.5 McFarland turbidity (108 × 1.5) was prepared and each well of the ELISA plate was filled with 100 mL of Muller-Hinton broth (MHB) and then 100 mL of iron oxide nanoparticles were poured in the first cast well; Afterward, 100 μL of this mixture was removed and transferred to the next well. This process continued to the last well. Finally, the concentrations of iron oxide nanoparticles (2000, 1000, 500, 250, and 125 μg/mL) were obtained (Khatami et al., 2017).

2.11.3 Antibacterial mechanism of Fe_3O_4 Nanoparticle

The main mechanism by which iron oxide nanoparticles showed antibacterial activity might be via oxidative stress generated by ROS. ROS, including superoxide radicals (O^{2-}), hydroxyl radicals (–OH), hydrogen peroxide (H_2O_2), and singlet oxygen ($^1O_2$), can cause damage to proteins and DNA in bacteria. Metal oxide (FeO) could be the source that created ROS leading to the inhibition of most of the pathogenic bacteria including *Staphylococcus aurous* (Behera et al., 2012). Some authors have demonstrated that the small size of

nanoparticles also can contribute to bactericidal effects. For example (Ansari et al., 2017), reported that the ultra-small size of nanoparticles may facilitate their diffusion through porin channels of the bacterial cell wall to exert their antibacterial action via destruction of the membrane integrity and intracellular damage.

3. MATERIALS AND METHODS

3.1. Apparatus and Instruments

The apparatus and equipment that were used during this research work were Uv-Vis spectrometer ($T80^{+}$- PG instrument), Diffuse reflectance spectroscopy(Uv-Vis DRS Elico SL-150 spectrophotometer), XRD(Shimadzu, XRD-7000S South Korea), FTIR (FTIR Perkin Elmer's spectrophotometer), SEM (Scanning Electron Microscopy), TGA(Thermogravimetric Analysis), electronic balance, oven, beaker, test tube, magnetic stirrer, thermometer, Whatman No.1, filter paper, measuring cylinder, pH-meter, spatula, Erlenmeyer flask, volumetric flask, the ceramic crucible, Buchner funnel, and bare magnet.

3.2. Chemicals and Reagents

Chemicals and reagent including Ferrous chloride tetrahydrate ($FeCl_2.4H_2O$, Sigma aldria, 99% purity), Ferric chloride hexahydrate ($FeCl_3.6H_2O$, Sigma aldria, 99% purity), Hydrochloric acid (HCl, Riedel dehaen,Germeny,37 % HCl), Sodium hydroxide (NaOH, Sigma aldria 99% purity), Ethanol (C_2H_5OH 99.8%, Fmd, Ethiopia), Potassium dichromate ($K_2Cr_2O_7$, Sigma aldria 99% purity), Sulfuric acid (H_2SO_4 ,Sigma aldria 98% purity) ,2,5 diphenylcarbazide, Distilled water and *Catha edulis* plant leaf were purchased and used as usual.

3.3 Sample Collection and Preparation

3.3.1. Collection of *Catha edulis* (Khat) Plant Leaves

Khat (*Catha edulis*) leaves were purchased from Adama local market, Oromia Region, in Ethiopia. The leaf samples were thoroughly washed several times with tap water followed by distilled water to remove extraneous matter. The cleaned Khat leaves were completely dried at room temperature in open air and under shadow for about two weeks (15 days) to remove any remaining moisture content from the leaves. The dried leaves of the *Catha edulis* plant were crushed by using an electrical grinding machine to produce a fine powder. Finally, the dried and ground sample was stored for further processing (Fig. 2).

Figure 2 Step involved in the collection of *Catha edulis* plant leaf

3.3.2. Preparation of *Catha edulis* Plant Leaf Extract

The extraction of the plant leaf part was carried out as follows. 3.0 g of the powdered leaves were placed into a 500 mL round bottom flask followed by the addition of 100 mL of distilled water. The flask containing the mixture was placed on a hot plate and the mixture was allowed to boil at 60 ℃ for about 2 hours. Then the boiled suspension formed in the solution was allowed to cool for about 15 minutes and was filtered twice by using Whatman's No 1 filter paper. Then the plant extract was kept for the synthesis of magnetite nanoparticles.

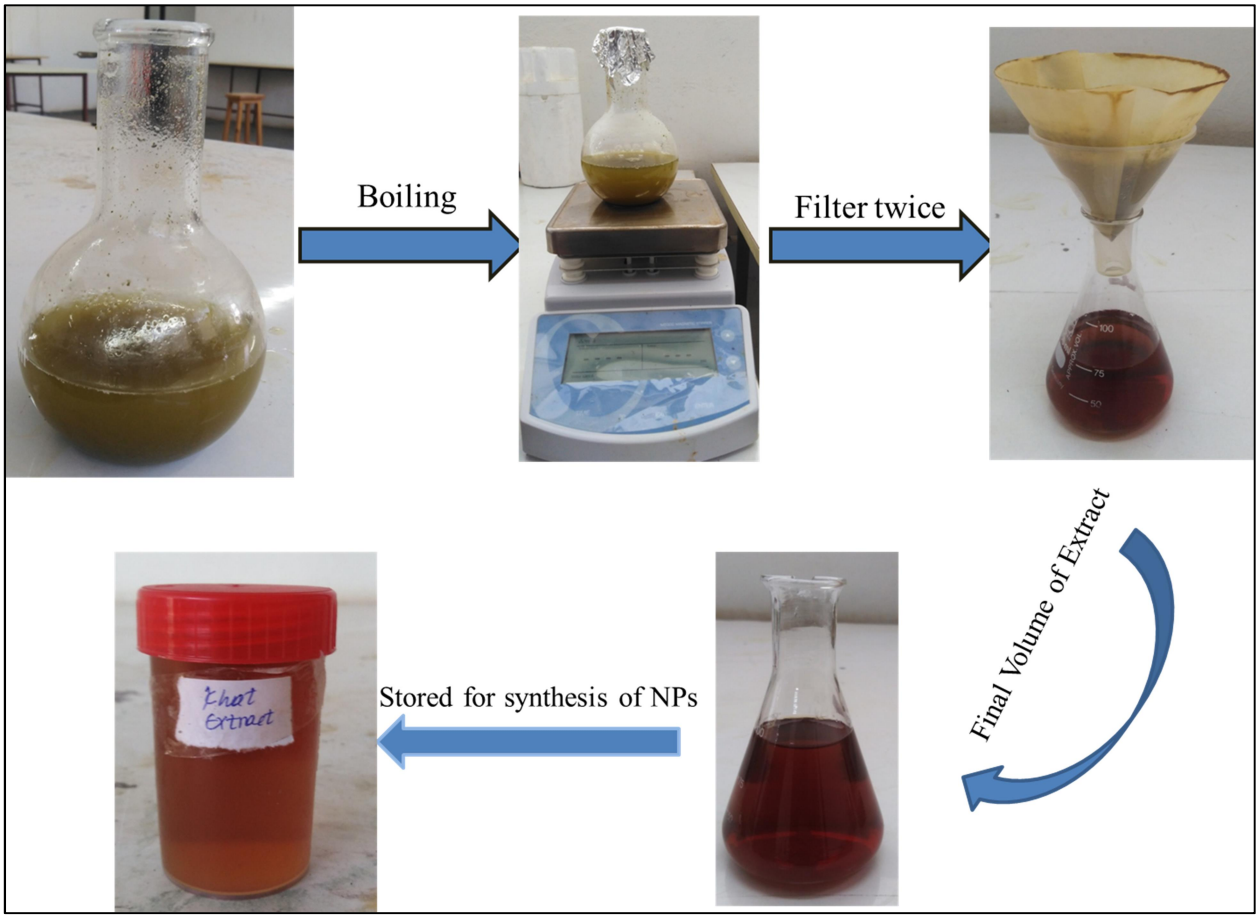

Figure 3 Steps involved in the preparation of *Catha edulis* plant leaf extract

3.3.3 Preliminary Phytochemicals Screening of *Catha edulis* Leaf Extract

The presence of alkaloids, glycosides, flavonoids, phenols, saponins, steroids, and tannins (gelatin) in the *Catha edulis* plant leaf extract were examined according to reported procedure (K. Gebremedhn et al., 2019).

3.3.3.1 Test for Alkaloids

1.2 g of iodine and 2 mL of H_2SO_4 were mixed and diluted into a 100 mL solution. Ten (10) mL of the alcoholic extract was acidified by adding 1.5% (v/v) of HCl and then a few drops of Wagner's reagent were added, and the yellow precipitate was formed to confirm the presence of alkaloids.

3.3.3.2 Test for Glycosides

A small amount of alcoholic extract was dissolved in 1 mL of distilled water and an aqueous NaOH solution was dissolved in 1 mL of distilled water and then it was added to the extract. The reddish-brown color was observed as an indicator of the presence of glycosides.

3.3.3.3 Test for Flavonoids

0.5 mL extract was added to 2 mL 10% (m/v) $FeCl_3$ solution and the mixture was shaken. A wooly brownish precipitate indicated the presence of flavonoid.

3.3.3.4 Test for Phenols

The Khat extract was treated with 3-4 drops of $FeCl_3$ solution. It was then left to form bluish-black color that indicates the presence of phenols.

3.3.3.5 Test for Saponins

0.2 mL extract was mixed with 5.0 mL distilled water, shaken for 20 min and the persistence of foams indicated the presence of saponins

3.3.3.6 Test for Steroids

2 mL of chloroform extract and 1 ml of concentrated H_2SO_4 acid were added carefully along the sides of the test tubes. The mixture was then examined to reveal a red color in the chloroform layer which confirms the presence of steroids

3.3.3.7 Test for Tannins

1.0 mL extract was stirred with 1.0 mL $FeCl_3$ solution; the occurrence of a greenish-black precipitate indicated the presence of tannins.

3.4 Synthesis of Magnetite NPs Using *Catha edulis* (Khat) Leaves Extract

3.4.1 Preparation of Precursor Salt Solution

The preparation of precursor salt solution was carried out by taking ferrous chloride and ferric chloride in 1:2 ratios respectively. Precisely, 2.65 g of ferrous chloride tetra hydrate ($FeCl_2 \cdot 4H_2O$) and 5.3 g of ferric chloride hexahydrate ($FeCl_3 \cdot 6H_2O$) were dissolved in 500 mL distilled water under mild magnetic stirring at 80 $^{\circ}$C on a hot plate. After 15 minutes, the light orange color appeared and then stored for further use. Then, three distinct samples were

prepared by mixing *Catha edulis* leaf extract in various volume ratios with precursor salts solution (Geneti et al., 2022).

3.4.2 Biogenic Synthesis of Magnetite NPs.

In a typical experiment, the extract was added to ferric chloride and ferrous chloride precursor solution in three different ratios by volume. For 1:1 ratio: 50 mL of ferrous chloride tetrahydrate, Ferric chloride hexahydrate, and 50mL of *Catha edulis* leaf extract, For 1:2 ratio: Ferrous chloride tetrahydrate, Ferric chloride hexahydrate 33.3 mL and 66.7 mL of . *Catha edulis* leaf extract and For 2:1 ratio: Ferrous chloride tetrahydrate, Ferric chloride hexahydrate 66.7 mL and 33.3 mL of *Catha edulis* leaf extract. Then after *Catha edulis* leaf extract were added while stirring on a hot plate. The solution turned brownish-black from orange and after 5 min, 100 mL of 1 M NaOH was added, and black precipitates of magnetite (Fe_3O_4) were prepared. Further, after 5 min of stirring, the solution was removed from the hot plate and left for settling down of iron oxide nanoparticles precipitates. Black precipitates of magnetite (Fe_3O_4) were washed five to seven times with distilled water and for drying, were placed in a hot air oven for 8 h at 80 ˚C (Fig-4). The prepared magnetite particles were stored in a tightly closed jar for characterization and experimental use (Altaf al., 2021).

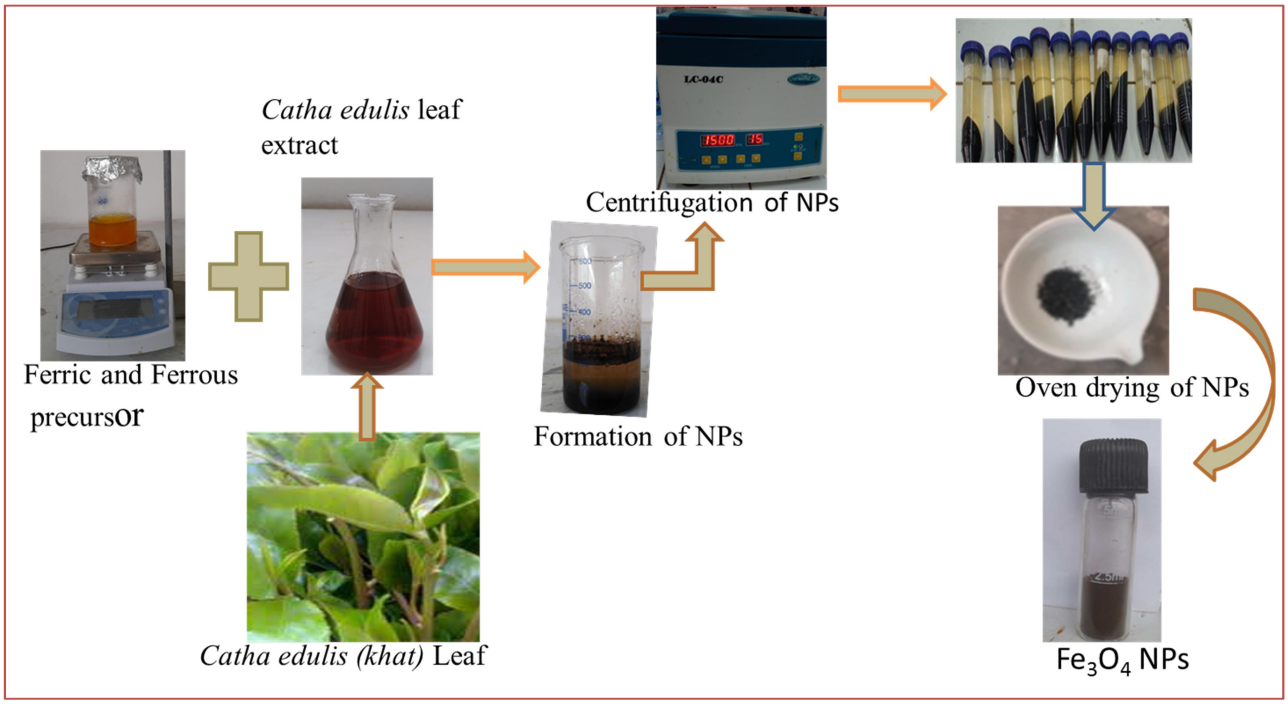

Figure 4: The schematic diagram of the synthesis procedure for Fe_3O_4 NPs

3.5. Characterization of Fe_3O_4 Nanoparticles

3.5.1 Characterization using X-ray diffractometer (XRD)

To determine crystallinity, structure imperfections, and crystallite size of the synthesized Fe_3O_4 Nps XRD were examined by using the Shimadzu XRD-700 X-ray diffractometer (XRD) at Adama Science and Technology University Material Science Department. The x-ray diffraction (XRD) patterns were recorded at the range of 2θ from 10 to 80 with a scan rate of 20/ min using Cu Kα (λ = 1.5406 A^0) radiation with an accelerating voltage of 40 KV. The crystallite size D of a particle can be estimated according to the Scherrer equation:

$$D = \frac{k\lambda}{\beta \cos \theta}$$

Here, the x-ray wavelength λ is 0.154 nm, k is the structure factor, which is assigned a value of 0.94, D is the average diameter of the crystals, θ is the Bragg angle in degrees, and β is the full-width at half-height of the prominent peaks (Gabal et al., 2022).

Sample Preparation: 1.5-2.5 gram of dried Fe_3O_4 NPs grinded by mortar and paste and then it was filled into the sample holder and subjected into X-ray diffractometer.

3.5.2 Characterization of Fe_3O_4 Nanoparticles Using Scanning Electron Microscope (SEM)

SEM analysis of the biosynthesized Fe_3O_4 NPs was carried out by using SEM (JCM-6000 plus BENCH TOP SEM, SHIMADZU Corporation, Japan) at Adama Science and Technology University Biology Department, which reveals information about the external morphology of the biosynthesized Fe_3O_4 sample with direct visualization.

Sample Preparation: A small amount of powder sample was dispersed in acetone and sonicated for a few minutes. Some samples need to be coated to make them conductive. Metals require no preparation because metal has the unique ability to conduct electricity. However, non-metals need to be coated with a conductive material such as gold/ gold-palladium alloy, using a sputter coater.

3.5.3 Characterization of Fe_3O_4 Nanoparticles Using Fourier Transform Infrared (FTIR)

FTIR analysis of the synthesized nanomaterials was done at Addis Ababa University Chemistry Department. FTIR spectrum of the dried powder of the biosynthesized Fe_3O_4 samples was recorded on 65 FT-IR (PerkinElmer) in the range 4000-400 cm^{-1}. FT-IR is used to identify the functional groups of the active components responsible for synthesizing Fe_3O_4 NPs (Mahdavi et al., 2013).

Sample Preparation: To create a very thin powder, the produced nanomaterial powders were combined with diluted potassium bromide (KBr). A thin, transparent pellet made from the powder was then squeezed, and this pellet was utilized to record the FTIR spectrum.

3.5.4 Characterization of Fe_3O_4 Nanoparticles Using UV-Vis Spectroscopy

The optical properties and band gap energy of biosynthesized magnetite nanoparticles were characterized by Uv-Vis DRS Elico SL-150 spectrophotometer at Addis Ababa University Chemistry Department. The range of absorption was between 200 nm to 800 nm.

Sample Preparation: A sample container with a rectangular or circular opening and a surface area of a few tens square millimeters to several square centimeters was carefully filled with finely ground standard ($BaSO_4$) and sample powder. The diffuse reflectance spectra were then taken after the holder was positioned horizontally at the base of the integrating sphere.

3.5.5 Characterization of Fe_3O_4 Nanoparticles Using Thermogravimetric analysis (TGA)

Thermogravimetric analysis of the biosynthesized Fe_3O_4 nanoparticles was done at Bahirdar University Chemistry Department in a flowing air atmosphere and the thermograms were recorded in the temperature range of 25–800 ^0C, at a heating rate of 20 ^0C/min. TGA measures the percent weight loss of a test sample.

Sample Preparation: A piece of powder specimen (7–8 mg) was placed in a platinum basket, and a thermocouple beneath the basket continually monitored the temperature. TGA calculates the percent weight loss of a test sample while it was heated evenly in the proper atmosphere.

3.6 Adsorption Study of hexavalent Chromium by Biosynthesized Fe_3O_4 Nanoparticles

3.6.1 Stock solution Preparation

The standard stock solution of chromium (1000 mg/L) was prepared by dissolving 2.829 g of 99.9 % analytical grade $K_2Cr_2O_7$ in 1000 mL of distilled water. Standard working solutions of chromium with different concentrations were prepared from the stock solution by appropriate dilutions. 20(mg/L), 30(mg/L), 40(mg/L), 50(mg/L) and (60mg/L of chromium standard solution were prepared by diluting 20(mg/L), 30(mg/L), 40(mg/L), 50(mg/L) and (60mg/L from 1000 ppm chromium stock solution with distilled water in 1000 mL volumetric flask up to the mark respectively. 1, 5-diphenylcarbazide was used for the spectrophotometric determination of Cr (VI). The pH of the aqueous solution was adjusted to the desired value by the addition of 0.1 M HCl or 0.1M NaOH solution (Husk, 2017).

3.6.2 Batch adsorption Experiments

Batch adsorption experiments were carried out at constant temperature T= 25± 2. The pH result was adjusted by using 0.1M of NaOH and HCl. The adsorption experiment was conducted by varying adsorbent dose (250mg – 1250mg), Cr^{6+} ion concentration (20−60 mg L^{-1}), agitation time (20min - 100 min), and pH (3, 5, 7, 9, 11). The solutions of Cr (VI) comprised of potassium dichromate ($K_2Cr_2O_7$) were taken into Erlenmeyer flasks. After pH was adjusted, a known quantity of adsorbent was added and finally, metal-bearing suspensions were kept under magnetic stirring. After shaking, the suspension was allowed to settle using an external magnet and the residual adsorbent with metal ions was filtered using Whatman filter paper, and metal ion concentrations in the filtrate were determined by UV-VIS spectrophotometer.

The percentage of Cr^{+6} ion removal and adsorption capacity was computed using equations 7 and 8, respectively

$$\text{Chromium removal (\%)} = \frac{(Co - \quad)}{Co} x\ 100 \qquad \text{..... (7)}$$

Where C_0 is the initial chromium ion concentration, C_e is the metal ion concentration at equilibrium, V is the volume of the solution, m is the mass of the adsorbent, and q_e is the adsorption capacity. Adapted from (R. Singh & Bhateria, 2020) with slight modification.

3.6.3 Adsorption kinetics Study

Adsorption kinetics is used to understand absorption mechanisms and the effect of contact time on adsorption. In each sample of 20 mg/L, 30 mg/L, 40mg/L, 50mg/L, and 60mg/L solution of hexavalent chromium, 1 g of magnetite was added followed by using a stirring rod at 100 rpm at pH =6-10. ml samples were taken after the following time intervals: 20 min, 40 min, 60 min, 80 min, and 100 min. Samples were filtered to remove magnetite particles and then diluted and measured using cuvette tests (Pandey et al., 2010).

3.6.4 Adsorption isotherm of hexavalent Chromium on magnetite

Equilibrium isotherms were obtained as follows. Several solutions with different known hexavalent chromium concentrations (20, 30, 40, 50, and 60 mg L^{-1}) were prepared and transferred to separate beakers. During continuous mixing on the stirring rod, 1g/L of magnetite was added to each sample. After stirring for 10 min the beakers were placed for 120 min to settle magnetite nanoparticles. Samples were taken from the upper clear part of the solution then diluted and equilibrium concentrations were measured using cuvette tests (Asfaw, 2021)

3.6.5 Desorption studies

Desorption studies employed 0.005 M solutions of NaOH eluents. Initially, metals were adsorbed on nanoparticles from 50 mL solutions containing 50 mg/L of metal ions. Then nanoparticles were striped using 20 mL of NaOH by agitating at 25 ^{0}C for 30 min. Then after a nanoparticle separated, the supernatant's metal ion concentration was analyzed. The adsorption-desorption cycles were repeated four times. The desorption efficiency was calculated using Eq. (8) (Rajput et al., 2016).

$$\text{Desorption efficiency (\%)} = \frac{\text{Released metal concentration}}{\textit{inintially adsrbed metal concentration}} \text{ x } 100 \qquad \ldots\ldots\ldots (8)$$

3.7 Procedures for Antibacterial Activity

The antibacterial activity of biosynthesized Fe_3O_4 by using (1:1, 2:1, and 1:2 ratios) of iron precursor salt and *Catha edulis* leaf extract were tested on four bacterial strains; (*S. aureus and S. pyogen*, *E. coli, and P. aeruginosa*) bacteria which were obtained from Microbiology laboratory of ASTU. Disc diffusion method was used for antibacterial activity of Magnetite (Fe_3O_4) nanoparticles.

3.7.1 Preparation of Inoculum

In four conical flasks, 25 mg of nutrient agar and 100 ml of distilled water were prepared and sterilized. In the first conical flask, *S. aureus* bacteria strain was inoculated, in the second conical flask *S. pyogen* was inoculated, in the third conical flask *E. coli* was inoculated and in the fourth conical flask, *P. aeruginosa* bacteria strain was inoculated and was kept in a rotary shaker for one day or 24 hours, 100 rpm.

3.7.2 Disc diffusion Method for Antibacterial Activity

A set of sterile discs (6 mm, Hi-media) impregnated with different concentrations of magnetite nanoparticles i.e. 50 µg/ disc (50µg/ml), 75 µg/ disc (75µg/ml), and 100 µg/ disc (100µg/ml), were prepared respectively, then culture plates were prepared by pouring 20 mL of Mueller- Hinton agar (Hi-media) medium and bacterial suspension swabbed on the medium plates using a sterile cotton swab and the plates were kept aside for few minutes. The discs were gently pressed and incubated in an inverted position for 24 hours at 37°C. The prepared dispersion solution was poured using a micro pipette of 20µL in each pathogen well. The plates were incubated at 37°C for 24 hours following which the antimicrobial activity was evaluated by measuring the zone of inhibition the obtained results were tabulated for evaluation (Manandhar et al., 2019)

4. RESULTS AND DISCUSSION

4.1 Phytochemicals Test of Catha *edulis* plant leaf extract

Phytochemicals screening is important as it gives information about the classes of compounds present in plant materials that might serve in reducing, capping, and stabilizing the nanoparticles. Based on the results, the naturally occurring phytochemicals in *Catha edulis* plant leaf extract were used as reducing and capping agents during magnetite nanoparticle synthesis.

The result of the phytochemicals test of *Catha edulis* is shown in Figure 5. It revealed the presence of secondary metabolites such as phenols, flavonoids, carbohydrates, tannins, alkaloids, etc. Therefore *Catha edulis* plant leaf extract is composed of phytochemicals which are capable of reducing the iron oxide by donating electrons, capping, and stabilizing the formed nanoparticles. For instance, biomolecules such as proteins, phenols, and flavonoids play a great role in reducing the ions to nanosize and also play an important role in the capping of NPs (Andualem et al., 2020)

The change formed during phytochemicals investigation is an indicator of the formation of different complexes as a result of oxidation and reduction reactions. For example, the yellow color of the alkaloid indicates that the nitrogen or oxygen atom of the amide groups of the alkaloids involve in a reaction. In most of the ferric chloride tests, the iron (III) ion forms complexes having different colors depending on the nature of the complexes (K. Gebremedhn et al., 2019).

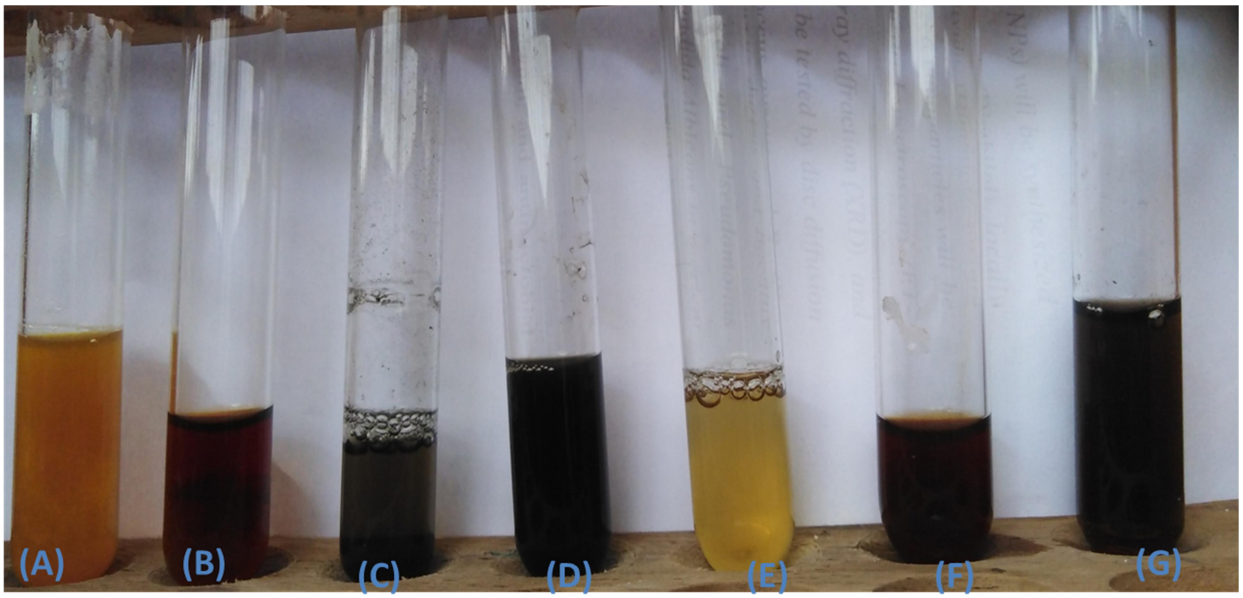

Figure 5: the color change observed when the leaf extract of Khat was tested for the presence of (A) Alkaloids, (B) Glycosides, (C) flavonoids, (D) Polyphenols, (E) saponins, (F) steroids, and (G). Tannins

4.2 Characterization of Fe_3O_4 NPs

4.2.1 Physical analysis

The light yellow color of $FeCl_2 .4H_2O$ and $FeCl_3 .6H_2O$ solutions were changed to light orange color upon string on the hot plate and also this light orange color started changing to brownish-black (Figure 6) as soon as *Catha edulis* plant leaf extract was added to iron salt precursor solution. These color changes indicate that the reduction is spontaneous for the formation of magnetite nanoparticles.

The brownish-black color observed could be the result of the interaction between the ion of iron precursor solution and biomolecules that are present in *khat* leaf extract, which leads to the spontaneous process of reduction. The biomolecules present in *Catha edulis* plant leaf extract consist of a phenolic ring and various electron-donating groups such as –OH, C=O, -OOH, etc. Through the mechanism of electron conjunction resonance and tautomerism, there is an increase in the availability of electrons for reduction to occur. In addition after sharing electron, the electron-donating group forms a covalent bond with iron particles which prevent

agglomerations of particle and impart stability to green synthesized magnetite nanoparticle (Dhar et al., 2021).

Figure 6: Color changes observed before and after the formation of Fe_3O_4NPs (A) ferrous and ferric chloride precursor, (B) leaf extract of Khat, and (C) Fe_3O_4NPs.

4.2.2 X-ray Diffraction (XRD) Analysis

Phase purity and crystallinity of synthesized magnetite nanoparticles can be identified by XRD analysis. Three samples were synthesized by three metals to plant extract ratios: (1:2), (2:1), and (1:1). The XRD pattern of these sample show similarity in the peak position and intensity distribution as can be seen in Figure 7a. The diffraction peak was observed for (1:2 ratio of Fe_3O_4 NPs) at 2θ = 30.23°, 35.45°, 43.27°, 53.7°, 57.1°, and 62.1°, which are corresponds to the crystal plane of (220), (311), (400), (422), (511) and (440).

Again as shown in Figure 7b (for the 2:1 ratio) diffraction peaks were found at 2θ values around 30.1°, 35.45°, 43.00°, 53.4°, 57.1°, and 62.7°, which could be assigned to crystal planes of (220), (311), (400), (422), (511) and (440). Similarly, for Fe_3O_4 (1:1) NPs (Figure 7c) diffraction peaks were observed at 2θ values of 30.23°, 35.4°, 43.1°, 53.4°, 57.0°, and 62.6°, which corresponds to a crystal plane of (220), (311), (400), (422), (511) and (440).

The diffraction patterns of Fe_3O_4NP was found to be in good agreement with JCPDS card number 00-019-0629, which confirms the formation of pure Fe_3O_4 NPs without the formation of any secondary phase. This implies that the green synthesized Fe_3O_4 nanoparticle possessed higher crystallinity, and no XRD detectable impurities were observed in this sample as well, which confirms the purity of the magnetite (Fe_3O_4) nanoparticle.

The crystal size of the green synthesized magnetite (Fe_3O_4) nanoparticle was calculated by using the Debye Scherrer equation. As a result of the crystal size of green synthesized magnetite (Fe_3O_4) nanoparticles corresponding to the highest intense peak (1:1), (2:1), and (1:2) were calculated and found to be 12.13 nm, 14.06 nm, and 9 nm respectively. The result showed that the plant extract was responsible for the reduction or capping of the nanoparticle. It was also observed that the size of the NPs decrease with increasing the amount of the plant extract.

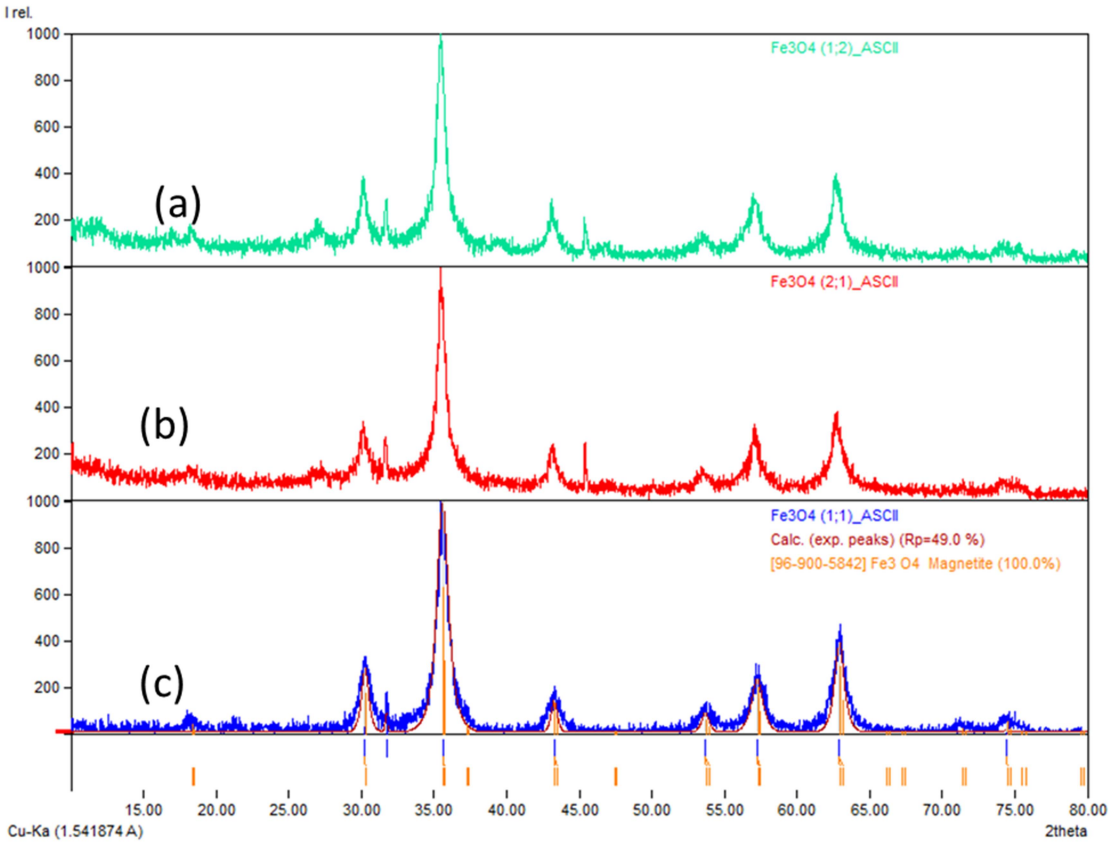

Figure 7 : XRD patterns of green synthesized Fe_3O_4 NPs using: (a) 1:1, (b) 2:1 and (c) 1:2 mass ratio of $FeCl_3$ and $FeCl_2$: plant extract.

Table 1 crystallite sizes of Biosynthesized Fe_3O_4 NPs.

Sample name	Peak position (2 theta)	FWHM (deg)	Crystal size D(nm)	Average D (nm)
Fe_3O_4 NPs (1:2)	30.273	0.9817	8.38322306	9.00
	35.6114	1.025	8.140462346	
	43.27	0.94	9.091881251	
	53.7	0.89	10.00476051	
	57.1	0.97	9.323753579	
	62.8809	1.025	9.084250451	
Fe_3O_4 NPs (2:1)	30.1564	0.6533	12.59383092	14.06
	35.5245	0.6943	12.01489922	
	43.1668	0.67	12.75122406	
	53.4767	0.46	19.33799693	
	57.0779	0.575	15.72711692	
	62.7134	0.78	11.92699099	
Fe_3O_4 NPs (1:1)	30.23	0.6233	13.20227077	12.14
	35.4	0.742	11.23860802	
	43.1	0.66	12.94144224	
	53.4	0.74	12.0168676	
	57	0.84	10.76160988	
	62.6	0.735	12.64959305	

4.2.3 Fourier Transform Infrared (FTIR) Analysis

FTIR spectra of Catha edulis plant leaf extract and green synthesized magnetite nanoparticle are presented in Figure 8 and Figure 9 respectively. Figure 8 shows the FTIR spectrum of *Catha edulis* plant leaf extract. The strong absorption peak at 3405 cm^{-1} indicates the –OH vibrational stretching of alcohol and phenolic compounds. A band at 2920 cm^{-1} reveals the C-H stretching of hydrocarbon. The peak at 2100 cm^{-1} is due to stretching vibration of alkenes or aromatic C=C bending. The peaks at 1431 and 1030 cm^{-1} corresponded to C-C weak stretching vibration of Alkane and C-O stretching bond. The existence of these biologically

active plant compounds might have been accountable for the reducing and capping of magnetite (Fe_3O_4) NPs. The presence of these functional groups indicated well capping and reduction of *Catha edulis* plant extract on the surface of nanomaterials. These results were similar to the previous report on the synthesis of magnetite (Fe_3O_4) NPs using different plant extracts (Kumar, 2019 and Yew et al., 2016).

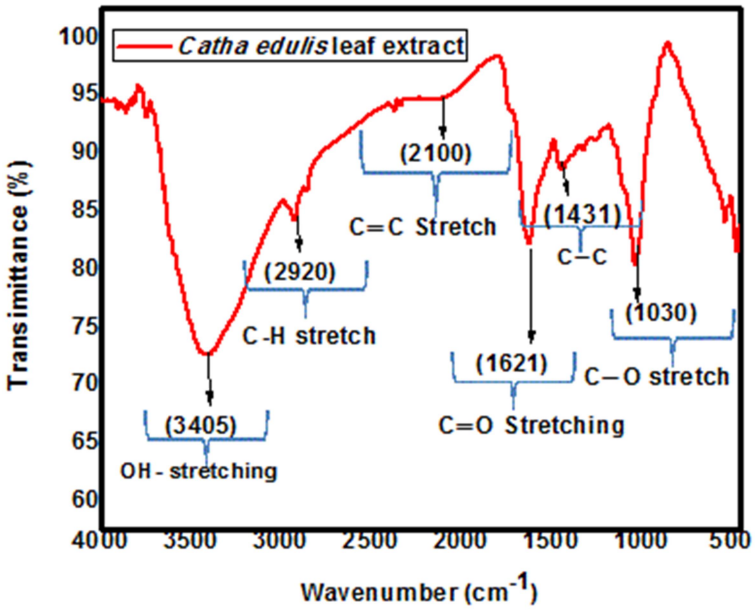

Figure 8 FTIR spectrum of *Catha edulis* plant leaf extract.

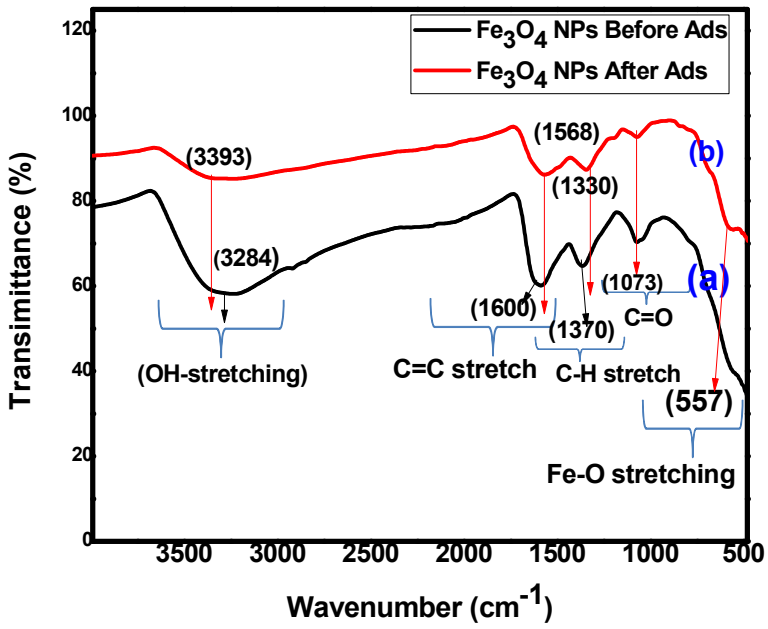

Figure 9: FTIR spectrum of green synthesized magnetite (Fe_3O_4) nanoparticles before adsorption (a) and after adsorption (b)

The FTIR spectrum of green synthesized magnetite nanoparticles before and after adsorption (Figure 9) Peaks at 3393 cm^{-1} and 3284 cm^{-1} could be assigned to the presence of alcohol, and phenol with O-H stretch. A band at 1569 cm^{-1} and 1600 cm^{-1} reveals the presence of carbonyl group C=C (1550-1650) (Gabal et al., 2022). A band at 1330 cm^{-1} and 1370 cm^{-1} corresponds to the C-H stretching of alky group. Peaks at 1073 cm^{-1} represent the stretching vibration of the carboxylate group (C=O). The peak formed around 1073 cm^{-1} is due to COO stretching vibration in carboxylic acid and flavonoids. The absorption band at 557 cm^{-1} corresponds to the Fe-O bonds.

According to Figure 9, no additional peaks in the FTIR spectrum of nanoparticles after adsorption have been generated. In fact, any chemical bond between chromium anions and nanoparticles has not been formed during the adsorption process. Thus, the adsorption mechanism of Cr(VI) onto Fe_3O_4 nanoparticles is suggested to be electrostatic attraction. So, the desorption process of nanoparticles may be useful for reusing of adsorbent (Jadidi et al., 2017) .

4.2.4 UV-Vis DRS analysis of biosynthesized Fe_3O_4 NPs

The band gap energy of the green synthesized magnetite nanoparticle by using *Catha edulis* plant leaf extract were analyzed by using diffuse reflectance measurement which is shown in Figure 10-12**.** The UV-Vis spectrum of green synthesized magnetite nanoparticles revealed the reduction process and formation of nanoparticles. Magnetite nanoparticle was confirmed by the immediate change in color of the reaction mixture from light yellow to dark brown after the addition of *Catha edulis* plant leaf extract, this was confirmed by the appearance of a strong peak at the range of 355–365 nm for each of the three-volume ratios of Fe_3O_4 NPs.

The band gap energy (E_g) of magnetite nanoparticles was calculated using Kubelka–Munk model. This model can be expressed in the following equation:

$$F(R) = (1-R)^2 /2R \quad \ldots\ldots\ldots\ldots\ldots\ldots\ldots\ldots\ldots\ldots\ldots\ldots\ldots\ldots\ldots\ldots\ldots\ldots\ldots \quad (9)$$

Where F(R) is the Kubelka-Munk function, and R is the reflectance. The bandgap represents the minimum energy necessary to excite an electron up to a state in the conduction band to take part in conduction (Gabal et al., 2022).

These band gap results show that the energy band gap of the Fe_3O_4 (1:2), Fe_3O_4 (2:1), and Fe_3O_4 (1:1) nanoparticles are 2.54 eV, 2.32 eV, and 2.4 eV respectively. Among the three nanoparticle ratios of Fe_3O_4 NPs, 1:2 volume ratios have larger band gap energy and this indicates that the energy bandgap of Fe_3O_4NP is associated with particle size. The smaller the particle size the larger the band gap. This can be explained quantum mechanically as the particle size reaches the nanoscale, the number of overlapping orbitals or energy levels decreases, and the thickness of the band becomes thinner. This causes a rise in the energy band gap between the valence band and the conduction band (M. Singh et al., 2018). Furthermore, this band gap value stated that Fe_3O_4 is an n- and p-type semiconductor with low resistivity owing to its minor bandgap in the range of 0.1–3.6 eV (Yusefi et al., 2021)

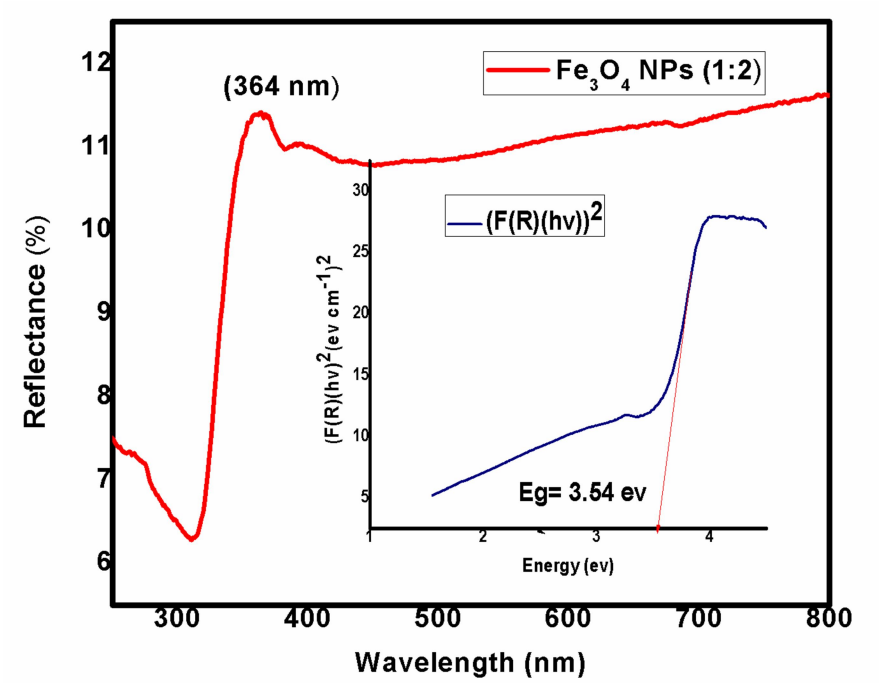

Figure 10: DRS spectra of green-synthesized Fe_3O_4 NPs (1:2) and its corresponding band gap energy

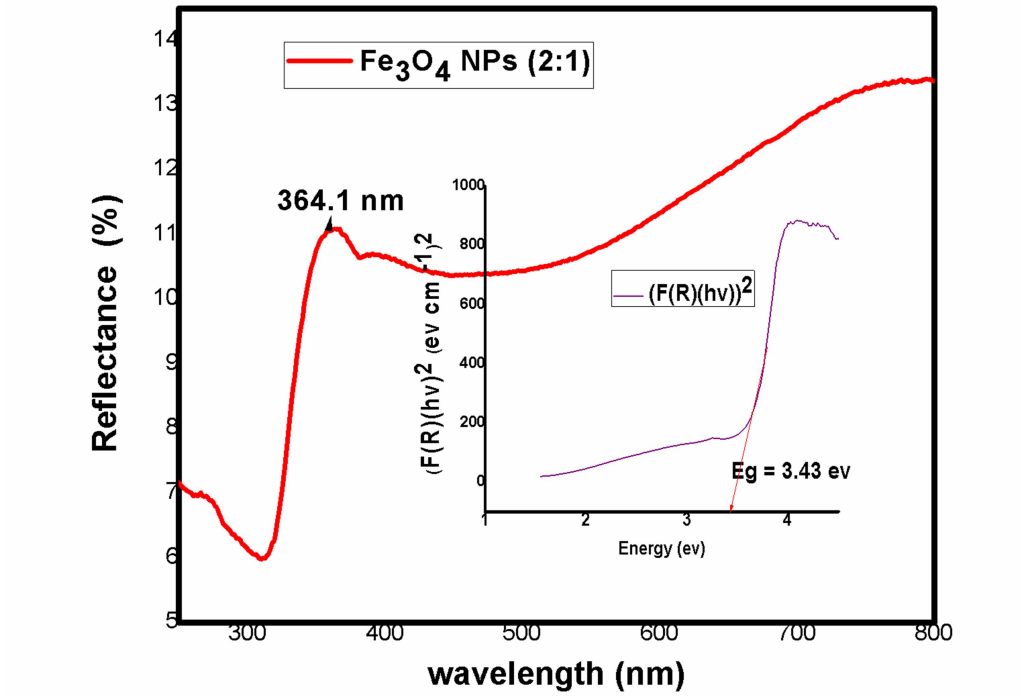

Figure 11: DRS spectra of green-synthesized Fe_3O_4 NPs (2:1) and its corresponding band gap energy

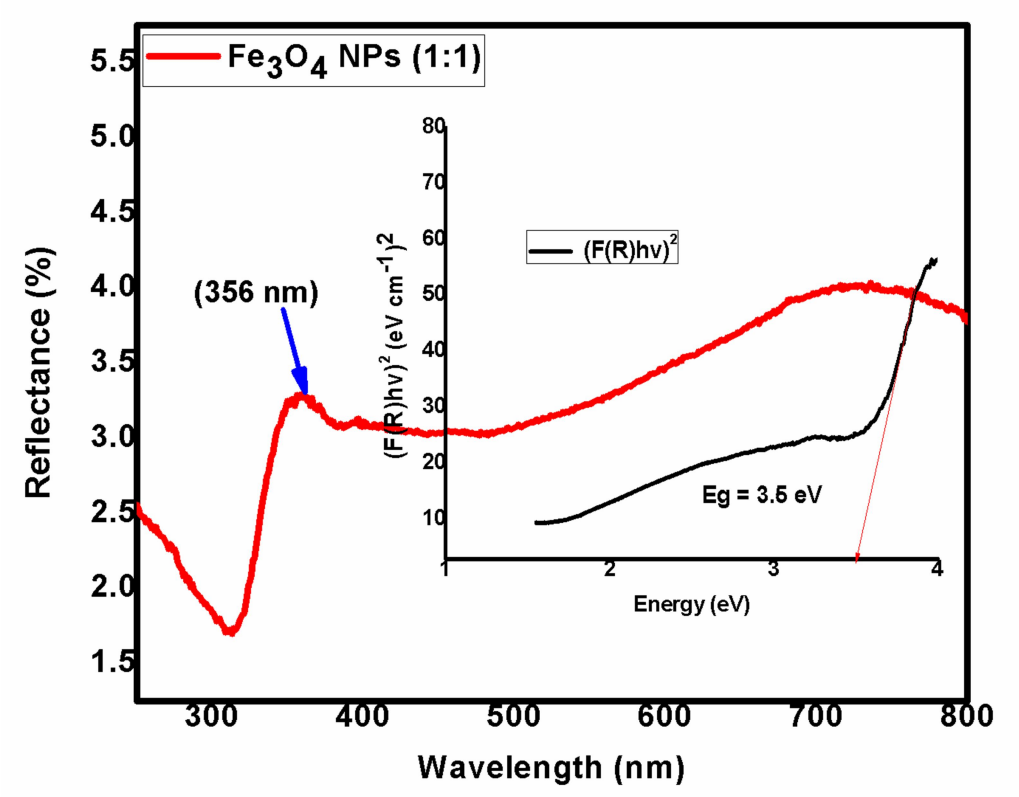

Figure 12: DRS spectra of green-synthesized Fe_3O_4 NPs (1:1) and it is corresponding band gap energy

4.2.4 Thermogravimetric analysis of biosynthesized Fe_3O_4 NPs

TGA analysis was done to study the thermal stability, decomposition temperature, and also decomposition rate of the nanoparticles. The TGA curve of magnetite (Fe_3O_4) is shown in Figure 13. The TGA plot reveals three weight loss steps in the tested temperature range which are associated with degradation of the main component of the nanoparticle. The first weight loss of about 0.95% happened and one exothermic peak of the DTA curve at 136 °C; indicating the removal of H_2O and organic moieties. In the second stage, two endothermic peaks observed at 267.6°C, 310.2°C, and 1.02% weight loss depicts the decomposition of the biomolecules from the plant extract. The temperature above which the weight loss became constant was used as the calcination temperature for the synthesized Fe_3O_4 nanoparticles. In the last step, there were no signs of any specific weight losses throughout the range of 450–

800°C, and exothermic peaks are observed in the DTA curve at 690.2°C. The calcination temperature is the temperature above which the weight loss of the sample is kept constant. Calcination was performed at 450 °C to remove unwanted plant extract residues and improve the purity of iron oxide NP (Geneti et al., 2022).

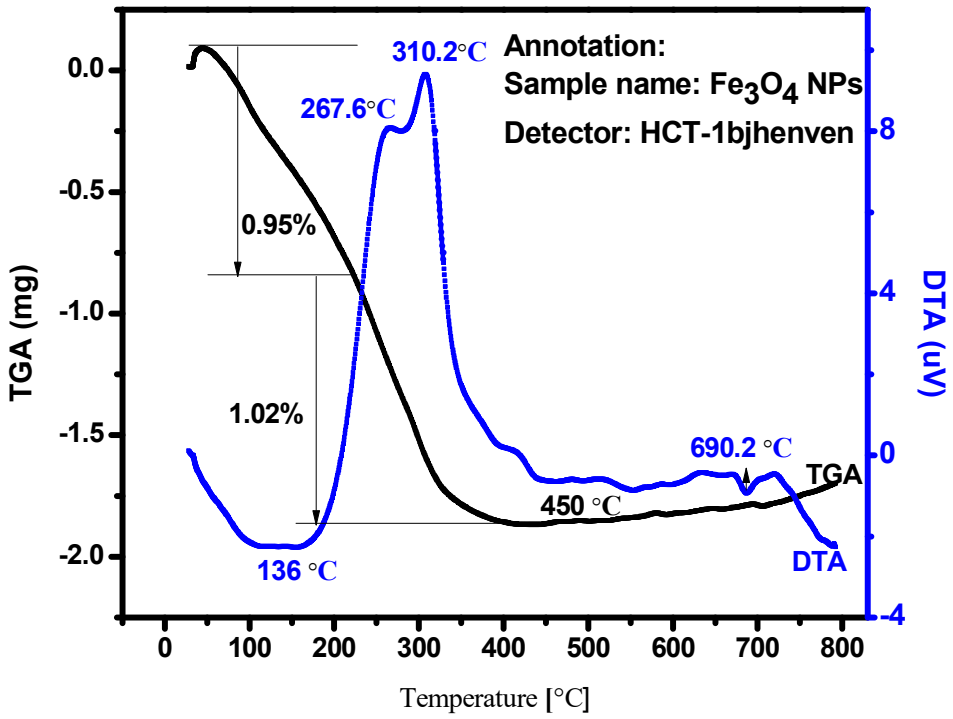

Figure 13: The TGA-DTA plots of green synthesized magnetite (Fe_3O_4) NPs

4.2.5 SEM analysis of biosynthesized Fe_3O_4 NPs

The surface morphology of the green-synthesized Fe_3O_4 NPs adsorbent was characterized by using scanning electron microscope (SEM). As shown in Figure 14, the SEM image before and after adsorption of Cr metal ions on the surface of the adsorbent material. The produced Fe_3O_4 NPs presented different morphologies and microstructural characteristics for Fe_3O_4 nanopowder, and also the image of Fe_3O_4 NPs presented the nanoparticle morphology are homogenous in structure, according to the SEM pictures.

The structure and morphology of Fe_3O_4 NPs adsorbent before adsorption showed variously sized and shaped vacant pores on the adsorbent. However, the Fe_3O_4 NPs surface showed a

reduction in the size of some pores, disappearance of some pores, disappearance of corners or edges, corrosion, and roughening after adsorption of the chromium. This confirmed that the pores of the adsorbent were filled with the hexavalent chromium ion and the surface has become puffy due to the resulting heterogeneity.

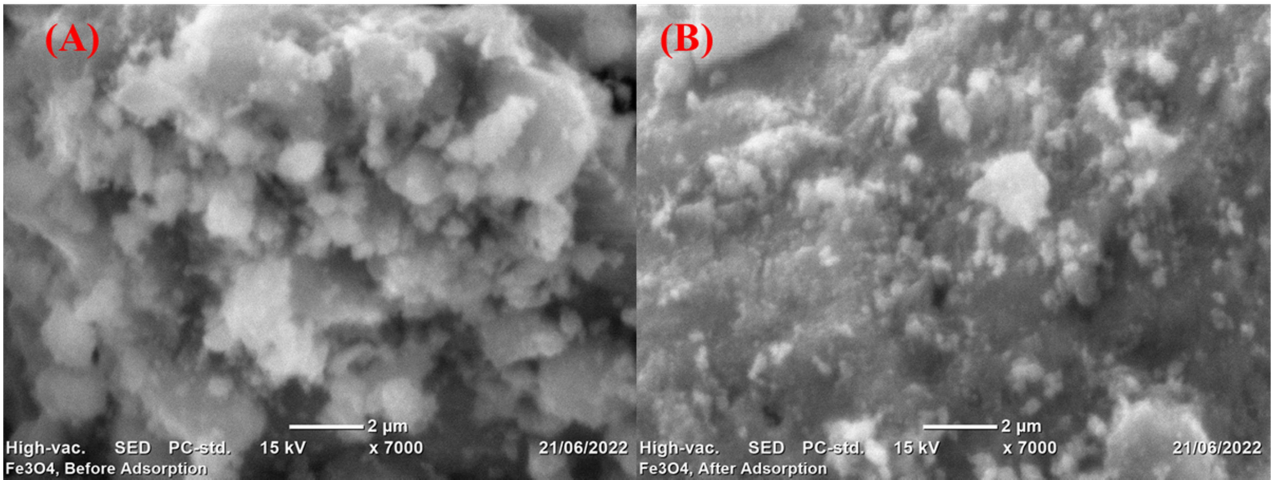

Figure 14: SEM images of: (a) Fe_3O_4 NPs before adsorption (b) Fe_3O_4 NPs after adsorption

4.3 Adsorption Batch Studies

Calibration curve for standard solution were done by various concentrations (10 mg/L, 20 mg/L, 30mg/L, 40mg/L). The experiments were repeated three times and the average data were used to plot the resultant graphs. A calibration curve of absorbance against chromium concentrations was plotted as seen in Figure 15. The experimental data reported in the Figure 15 were fitted by a straight line with a high regression coefficient value (R^2= 0.99986)

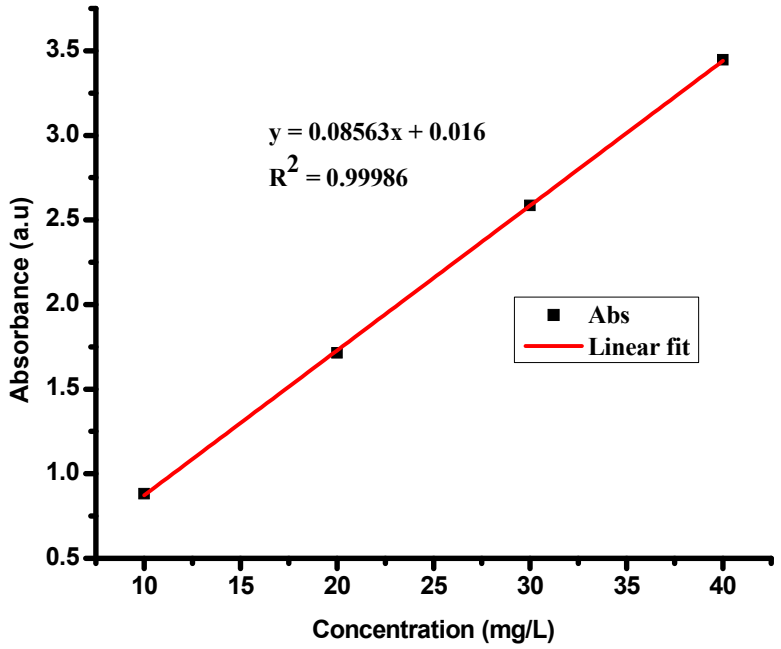

Figure 15: Calibration Curve for standards Samples

4.3.1 Optimizer Design of Different Parameters

The optimization was done considering different ratios of nanoparticle to get which ratio of the nanoparticle can have maximum % removal of chromium. At initial concentration of 20 mg/L, maximum removal of 97.2% (1:1 Fe_3O_4 NPs), 96.9 % (2:1 Fe_3O_4 NPs) and 98.2% (1:2 Fe_3O_4 NPs) of chromium was achieved with three ratio of Fe_3O_4 NPs by keeping other parameters constant (pH =3, adsorbent dosage =1000 mg, contact time = 90 min).

From the synthesized magnetite (Fe_3O_4) nanoparticles by using *Catha edulis* plant leaf extract which is synthesized by three different ratios (1:1), (2:1) and (1:2) of iron precursor to *Catha edulis* plant leaf extract solution. As the particle size was found to be smaller in the case of 1:2

ratio, all the parameter optimizer designs of adsorption were done on the best sample of Fe_3O_4 (1:2) NPs for removal of Cr (VI), with the expectation that adsorption efficiency was higher than the other samples which at the end became a reality.

4.3.2 Factors Affecting the Adsorption

4.3.2.1 Effect of pH on Adsorption

The pH of the aqueous solution is one of the important factors that controlled the adsorption process. The experiments of this stage were performed under the conditions of constant contact time (60 min), adsorbent dose (1000 mg), initial chromium concentration (20 mg/L), and various pH values from 3 to 11 were selected for the experimentation. The pH of the solution was regulated by using 0.1 M HCl or 0.1 M NaOH solutions and the chromium removal was investigated. The experimental results (Figure 16**)** revealed that the removal efficiency of adsorbent Fe_3O_4 NPs was increased from pH 3 to 5 Fe_3O_4 NPs exhibited the highest percent removal (98.5%) of chromium (VI) at a pH value of 5 and by increasing pH, a drastic decrease in adsorption percentage was observed. This might be due to the weakening of the electrostatic force of attraction between the oppositely charged adsorbate and adsorbent ultimately leading to the reduction in sorption capacity (Nameni et al.,2008).

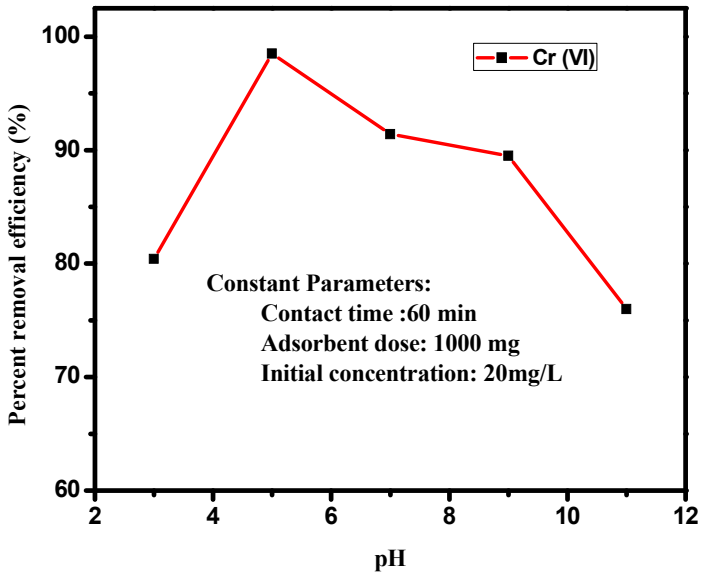

Figure 16: Effect of pH on the Cr ion adsorption by magnetite nanoparticles

4.3.2.2 Effect of Adsorbent Dosage

The effect of adsorbent dosage on the removal of Cr (VI) ion from the standard working solution of Cr (VI) concentration was studied. Figure 17 revealed that the percentage removal of Cr (VI) ion was increased from 75.4 % to 98.6 % as the amount of adsorbent dosage was also increased from 250 mg to 1250 mg. This result could mainly explain the influence of available adsorption sites on removal efficiency as increasing the adsorbent dose was found to increase the number of the active site available for adsorption. An increase in adsorption with dose can be attributed to increased surface area and the availability of more binding sites for adsorption (Edris et al., 2019)

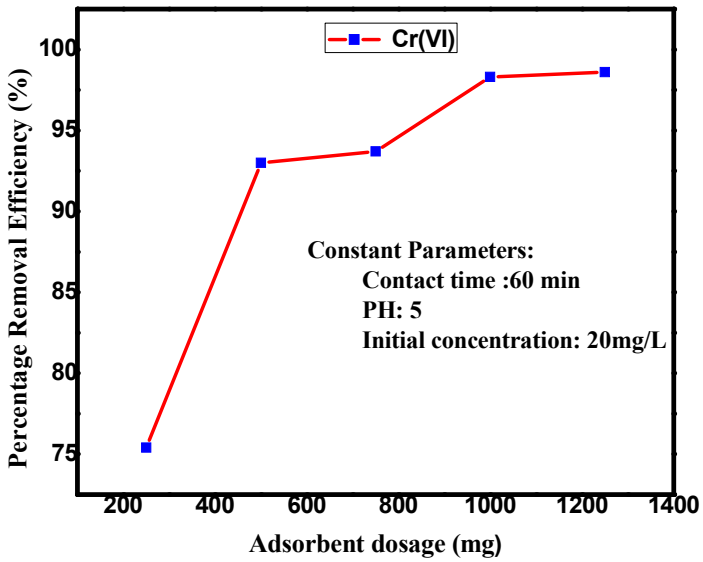

Figure 17: Effect of adsorbent dosage on the Cr ion adsorption by magnetite nanoparticles

4.3.2.3 Effect of Contact Time

The Cr(VI) adsorption experiments were carried out for different contact times with fixed adsorbent dose, pH, and initial concentration. The effect of contact time on the adsorption efficiency of the Fe_3O_4 NPs with 30 mg/L of hexavalent chromium ion concentrations, pH=5, 1000 mg adsorption dose, and contact time (20 min,40 min,60 min,80 min, and 100 min). According to the result presented in figure 16, the removal efficiency was increased in the beginning but it was decreased till reaching the equilibrium. As shown in Figure 18 the

optimum contact time for adsorption of Cr (VI) ion by using Fe_3O_4 NPs was 60 minutes with a percentage removal of 96.1%. It is easy for chromium to access the active adsorption site, thus resulting in a rapid uptake of chromium. However, with an increase in contact time, the system attains a steady state. After that, the occupancy of other remaining vacant sites is difficult because of the repulsive force between chromium ion adsorbed on the surface and adsorbate in the solution

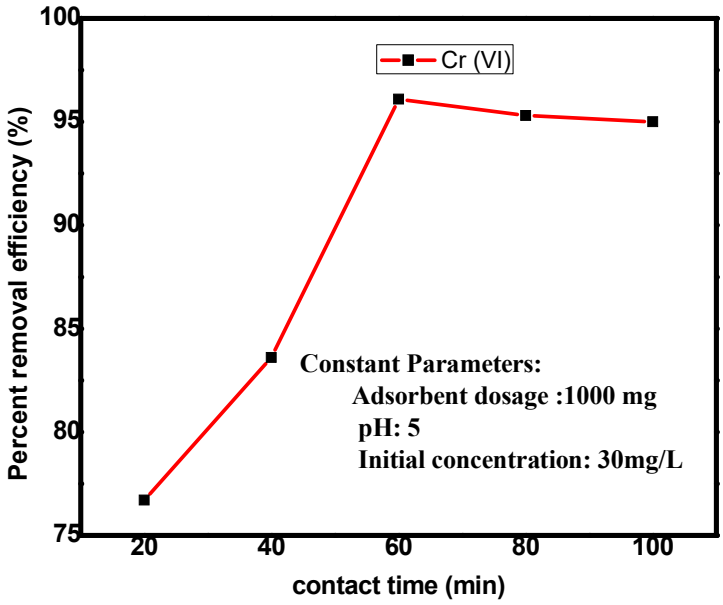

Figure 18: Effect of Contact Time on the Cr ion adsorption by magnetite nanoparticles

4.3.2.4 Effect of Initial Concentration on Adsorption of Chromium

The effect of different initial chromium concentrations (20, 30, 40, 50, and 60 $mg \cdot L^{-1}$) on the removal efficiency of chromium was studied, by keeping all the other parameters constant (at pH =5, contact time =90 min, and absorbent dosage =1000 mg. as shown in Figure 19 the chromium adsorption capacity was decreased from 98.6% to 64.8% with an increase in the initial concentration of Cr (VI) from 20mg/L to 60mg/L. On the other hand, the removal efficiency of Cr (VI) is higher at lower Cr (VI) concentrations with further residual Cr (VI) ions remaining in the aqueous solution. This can be explained by the fact that all the adsorbents had a limited number of active sites, which would have become saturated above a

certain concentration. For instance, a decrease in the percentage of removal with increasing initial concentration of chromium ion in this study is that as the ratio of chromium ion to Fe_3O_4 NPs increases, the exchangeable sites in Fe_3O_4 NPs structure are saturated, resulting in a decrease of the removal percentage.

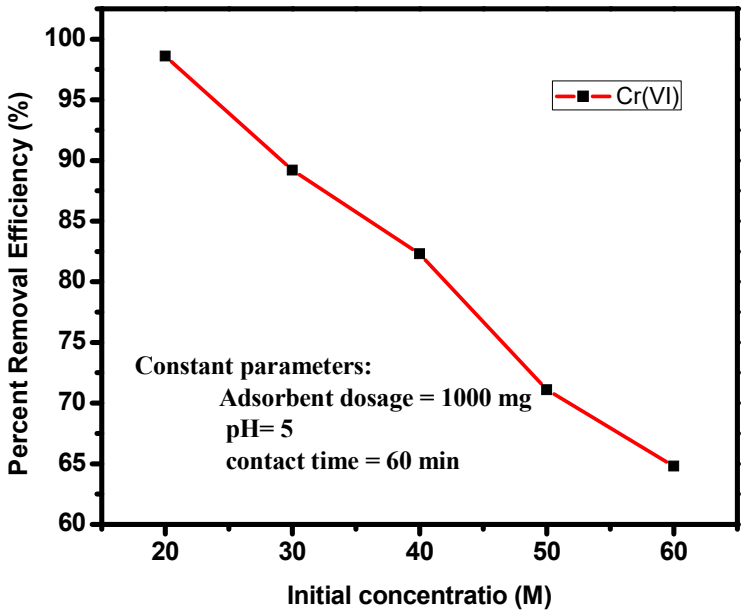

Figure 19: Effect of Initial concentration on the Cr ion adsorption by magnetite nanoparticles

4.3.3 Adsorption kinetics Study

An adsorption kinetics study is an important tool for analyzing the adsorption process of Cr (VI) on the surface of Fe_3O_4 nanoparticles was conducted against two common kinetic models such as pseudo-first-order and pseudo-second-order.

4.3.3.1 Pseudo-first Order Kinetic Model

Pseudo-first order kinetics is determined under the following equation 10

$$\ln (q_e - q_t) = lnq_e - K_1 \text{ x } t \quad \text{..... (10)}$$

Where qe (mg/g) and qt (mg/g) are the mass of metal adsorbed at equilibrium and at time t, respectively. K_1 is the first-order rate constant of adsorption. A straight line of log (q_e-q_t) versus t suggests the applicability of this kinetic model (Figures 20). q_e and K_1 were

determined from the intercept and slope of the plot, respectively (Table 3). The value of q_e and K_1 was found to be 3.9474 and -0.00022 respectively for Cr(VI). The R^2 values for this model at the studied concentration were 0.67866 for Cr (VI), as indicated in table 3. The low correlation coefficient values from the pseudo-first-order kinetics model indicate that adsorption does not occur at only one site per ion.

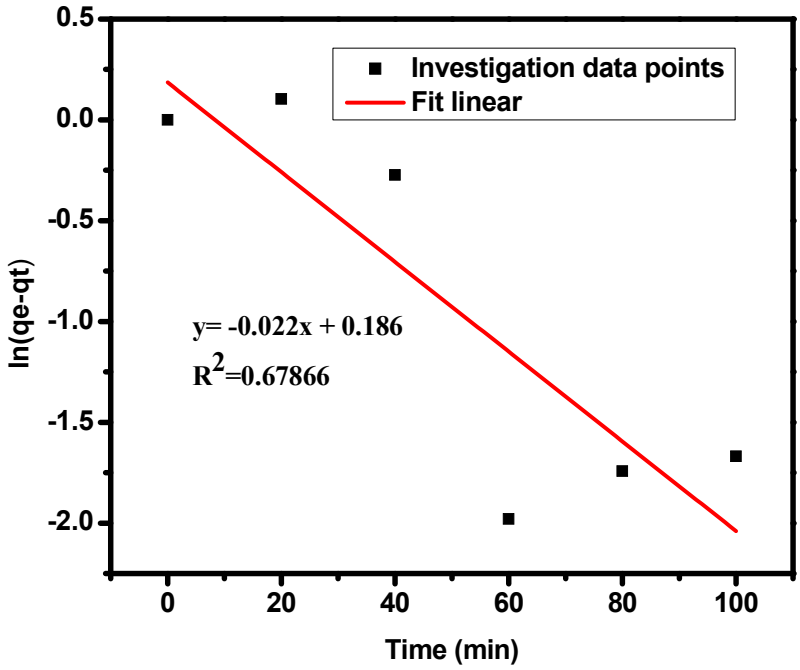

Figure 20: Pseudo first-order adsorption kinetics of Cr(VI) on magnetite nanoparticles with the same concentrations.

4.2.3.2 Pseudo-second Order Kinetic Model

Pseudo-second order kinetics are determined by the following equation 11

$$\frac{1}{qt} = \frac{1}{k2\ qe^2} + \frac{1}{qe * t} \quad \text{..... (11)}$$

Where, q_t is the metal uptake per unit weight of adsorbent (mg/g) at time t, qe is the metal uptake per unit weight of adsorbent (mg/g) at equilibrium, and k_2 (g/mg.min) is the rate constants of pseudo-second-order kinetics equations. The value of qe(mg/g) and K_2 (g/mg min) were obtained from the slope and intercept of the plot of t/q_t vs t described in Figures 21

and were found to be 10.67773 and 6.19778 respectively. The calculated equilibrium adsorption capacity values q_e (calc), of pseudo-second-order kinetic, were found to be 3.25849. The regression coefficient value (R^2) of the pseudo-second-order kinetic model (0.98188) was found to be higher than that of the pseudo-first-order kinetic model (0.67866). Figure 21 and Table 2: depict that the regression coefficient value is greater for pseudo-second-order kinetics than pseudo-first-order kinetics, confirms that the adsorption obeys the pseudo 2nd order adsorption process. The fact that the obtained result revealed the rate-controlling step of Cr (VI) adsorption on Fe_3O_4 NPs mediated by chemical sorption (chemisorption) and the sorption capacity is proportional to the number of active sites on the sorbent (Marcu et al., 2020)

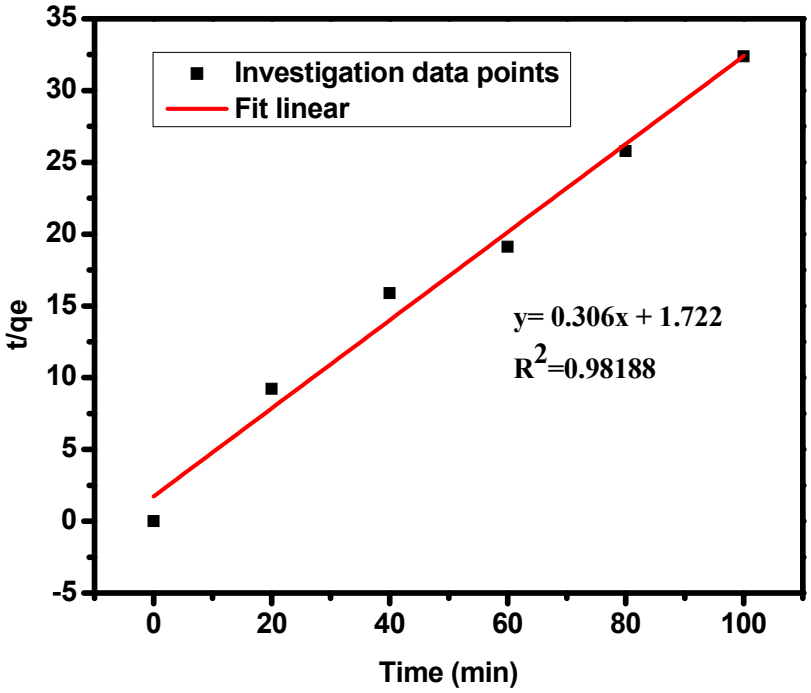

Figure 21: Pseudo-second order adsorption kinetics of Cr (VI) on magnetite nanoparticles with the same concentrations.

Table 2: Adsorption kinetics constants at the same concentrations

Metal ions	**Pseudo 1st order kinetic model**				**Pseudo 2nd order kinetic model**			
Cr (VI)	qe(mg/g)	qe_1	k_1	R^2	qe(mg/g)	qe_2	K_2	R^2
	1.20462	3.9474	-0.00022	0.67866	3.25849	10.67773	6.19778	0.98188

4.3.4 Adsorption isotherms Study

Adsorption isotherms are mathematical models that describe the distribution of metal ions between the liquid phase and the solid phase, based on a set of assumptions that are mainly related to the heterogeneity/homogeneity of adsorbents, the type of coverage, and the possibility of interaction between the adsorbate species. The most widely used isotherm equations are Langmuir and Freundlich's isotherm models.

4.3.4.1 Langmuir Isotherm Model

The Langmuir model assumes that the uptake of metal ions occurs on a homogenous surface by monolayer adsorption without any interaction between adsorbed ions. The Langmuir isotherm is represented by

$$\frac{C_e}{q_e} = \frac{K_L C_e}{Q_m} + \frac{1}{Q_m} \quad \text{.....12}$$

where Ce (mg/l) is the concentration of adsorbate left in solution at equilibrium, K_L is the Langmuir binding energy, Qm(mg g^{-1}) is the adsorption maximum (mg g^{-1}) and qe(mg g^{-1}) is the amount of adsorbate adsorbed per unit mass of adsorbent.

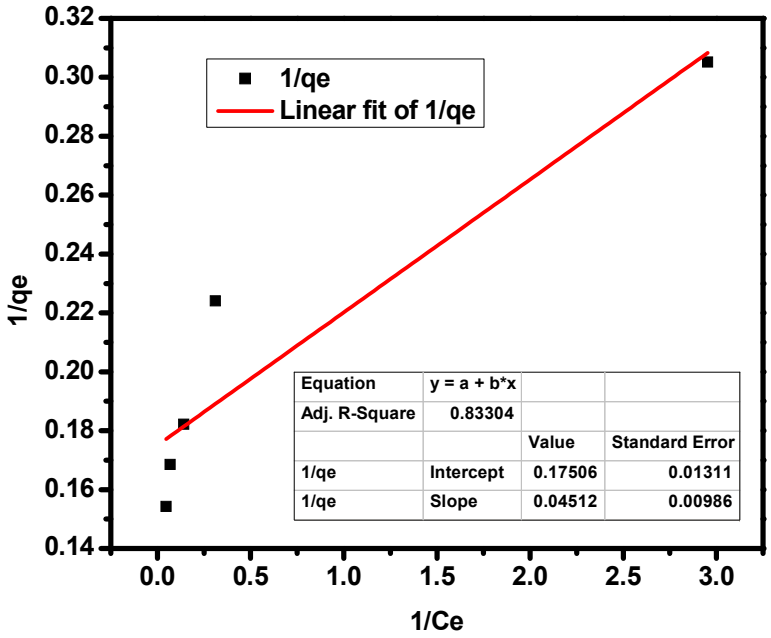

Figure 22: Langmuir isotherm model for Cr

Table 3: Langmuir isotherm model constants and correlation coefficients for adsorption of chromium

Langmuir isotherms of Cr (VI)						
Estimated isotherm parameters	Intercept	Slope	q_{max} (mg/g)	K_L	R_L	R^2
	0.58657	0.16524	1.704826	3.549806	178.4903	0.83304

4.3.4.2. Freundlich Isotherm Model

The monolayer adsorption of metal ions on a heterogeneous surface is what the Freundlich model predicts will happen (Nameni et al., 2008). Adsorption activities that take place on heterogeneous surfaces are subject to Freundlich isotherm. An expression for the surface heterogeneity and the exponential distribution of active sites and their energy is provided by this isotherm (Ayawei et al., 2017). The suitability of the isotherm was verified via the equation (13)

$$\text{Log } q_e = \log K_f + \frac{1}{n} \log C_e \quad \text{..... (13)}$$

Where q_e denotes the quantity of adsorbed Cr (VI) per quantity of adsorbent at the conditions of equilibrium (mg/g), Ce denotes the equilibrium concentration (mg/L), and K_f denotes the capacity of adsorption, and n denotes the intensity of adsorption.

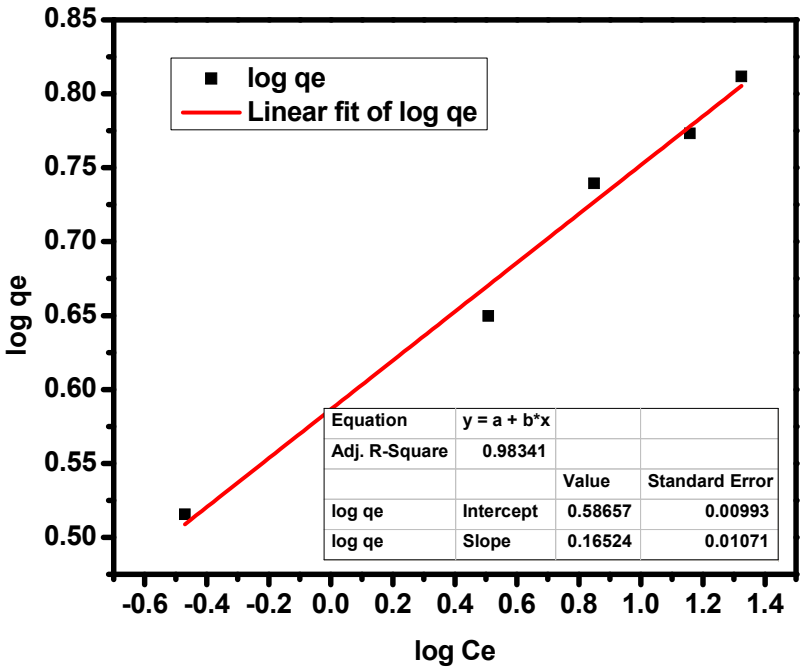

Figure 23: Freundlich isotherm model for Cr

Table 4: Freundlich isotherm model constants and correlation coefficients for adsorption of chromium

Freundlich isotherms of Cr (VI)					
Estimated isotherm parameters	Intercept	Slope	1/n	K_f	R^2
	0.58657	0.16524	0.16524	3.859846	0.98341

Figures 22 23, and Table 3, and 4 display the linear adsorption isotherm plot and associated fitting parameter. The outcome shows that utilizing the linear versions of the isotherm

equations, the Freundlich model (R^2 = 0.9834) is better suited to adequately represent the examined sorption phenomenon than the Langmuir model (R^2 = 0.83304). Thus, it is suggested that multilayer adsorption of Cr(VI) occurred on the heterogeneous surface of the magnetite nanoparticle.

4.3.5 Desorption Study

Desorption studies were conducted to investigate the use of adsorbent material repeatedly and economically. Adsorbent reusability was checked by conducting four adsorption-desorption Cycles. The recycled Fe_3O_4 NP has been tested against the removal of Cr(VI) metal ions for the 1st,2nd,3rd, and 4th cycles, respectively (Figure 24). The data of the regeneration study of Fe_3O_4 NP against Cr (VI) metal ions for the 1st four cycles are shown in Figure 24. The regeneration cycles of the magnetic nanomaterial's showed a slight decrease (about 7.86 % for Cr (VI) ions) in the removal efficiency between the 1st cycle and 4th cycle, indicating that the nanomaterial was reused for up to 4 cycles sequentially without significant reduction in removal efficiency of Fe_3O_4 NPs against Cr (VI) metal ions.

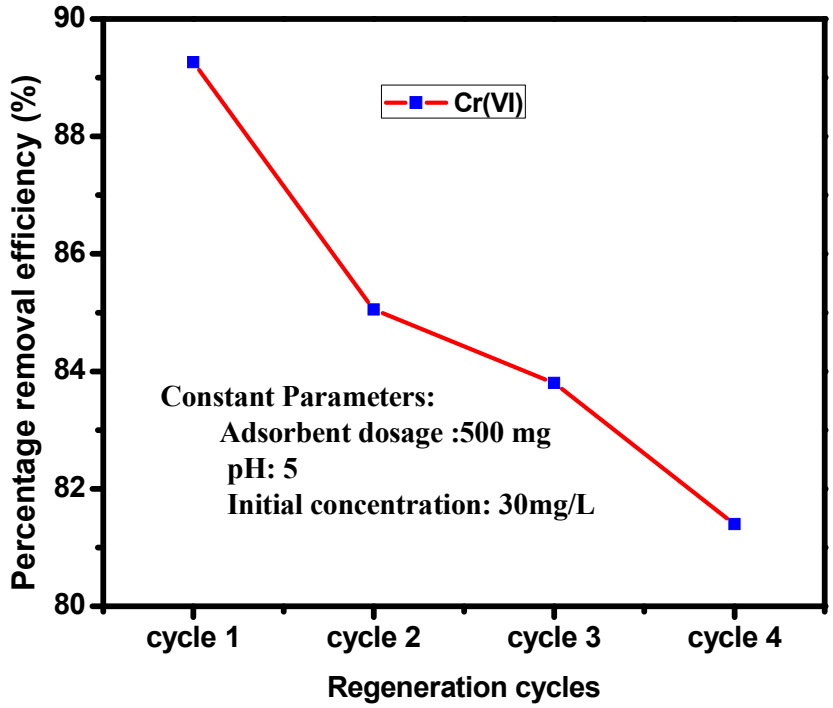

Figure 24: Regeneration experiment repeated up to four cycles

4.4 Antibacterial Activity of Fe_3O_4 Nanoparticles

The antibacterial activity of biosynthesized Fe_3O_4 Nanoparticles was tested by using the disc diffusion method against gram-positive and gram-negative bacteria strains. The antibacterial activity of Fe_3O_4 Nanoparticles was compared with the positive control Ampicillin: the results of antibacterial studies recommend that Fe_3O_4 Nanoparticles synthesized by using the ratio of ferric chloride hexahydrate and ferrous chloride tetrahydrate as a precursor and *Catha edulis* plant leaf extract in 1:1, 1:2 and 2:1 ratios as potential antibacterial agents. Fe_3O_4 nanoparticles synthesized by using the (1:2) ratio for all concentrations showed high antibacterial activity against all bacteria strains compared to Fe_3O_4 Nanoparticles synthesized by using the (1:1) and (2:1) ratio. This is most probably due to the small size it possessed compared to others which led to high penetration ability and caused fast cell damage. Moreover, as the concentration of Nanoparticles increased, the antibacterial activity of these nanoparticles was also enhanced similar to the previous report (Andualem et al., 2020).

According to the result presented in Table 5 and Table 6, the maximum inhibition zone was recorded for Staphylococcus aurous in 100ug/mL concentrations of Fe_3O_4 (1:2) ratio was found to be 12 mm followed by *S. pyogen and E.coli* of 11mm for both. 100ug/mL concentrations of Fe_3O_4 (1:1) nanoparticles showed very good activity against *S. aureus, S. pyogen,* and *E. coli as* their zone of inhibition was found to be 11.5 mm, 10.5 mm, and 10 mm respectively and also Fe_3O_4 (2:1) nanoparticles showed good activity against *S. pyogen, P. aeruginosa and S. aureus* as their zone of inhibition are found to be 10 mm, 9.5mm and 9mm respectively.

The result of this study also revealed that the Fe_3O_4 Nanoparticles showed a high antibacterial activity response on gram-positive (*S. aureus and S. pyogen*) bacteria than gram-negative (*E. coli and P. aeruginosa*) bacteria. This might be because gram-positive bacteria haven't outer membrane but rather are surrounded by a layer of peptidoglycan many times thicker than the other which is found in gram-negative bacteria.

Mechanistically, Fe_3O_4 nanoparticles exert their antibacterial action through the interactions of ferric ions with the proteins and DNA thereby causing the conformational changes in protein structure and DNA molecule, which ultimately leads to the mortality of bacterial cells (Ansari et al., 2017). Another proposed mechanism might be via oxidative stress ROS, including

superoxide radicals (O^{2-}), hydroxyl radicals (–OH), hydrogen peroxide (H_2O_2), and singlet oxygen ($^1O_2$), which can cause damage to proteins and DNA in bacteria. In this case, iron oxide could be the source that created ROS which may cause intracellular damage leading to a powerful bactericidal action (Behera et al., 2012). Generally in this study Fe_3O_4 nanoparticles synthesized by the green method show the effective antibacterial activity on both gram-negative and gram-positive bacterial strains.

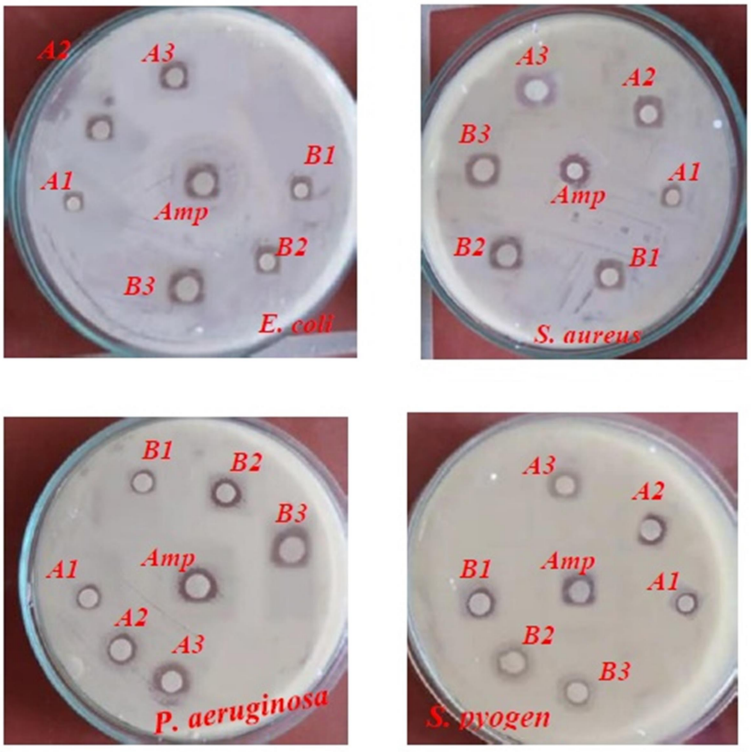

Figure 25: Antibacterial activity of (2:1) and (1:1) ratio of Fe_3O_4 nanoparticles.

Table 5: Zone of inhibition for A (2:1) and B (1:1) ratio of Fe_3O_4 nanoparticles on selected pathogenic bacterial strains

Cpd Conc. (Fe_3O_4)		**Bacteria Species and Zone of Inhibition**			
		***E. coli* ATCC25922**	***S. aureus* ATCC25923**	***P. aeruginosa* ATCC27853**	***S. pyogen* ATCC19615**
1:1	A1 50 µg/ml	7	8	7	8
	A2 75 µg/ml	9	10	8.5	9
	A3 100 µg/ml	10	11.5	9	10.5
2:1	B1 50 µg/ml	7	6	7	7
	B2 75 µg/ml	8	8	8	9
	B3 100 µg/ml	8	9	9.5	10
	Ampicillin (+ve control)	12	13	12	13.5

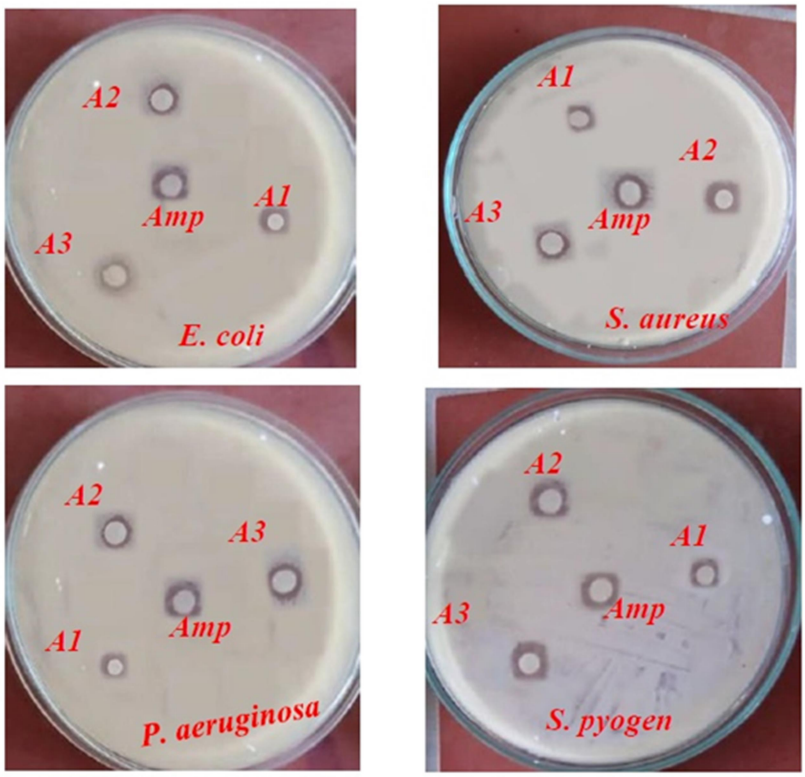

Figure 26: Antibacterial activity of Fe_3O_4 (1:2) nanoparticles.

Table 6: Zone of inhibition for (1:2) ratio of Fe_3O_4 nanoparticles on selected pathogenic bacterial strains

Cpd concentration (Fe_3O_4)		Bacteria Species and Zone of Inhibition			
		E. coli ATCC2592	*S. aureus* ATCC25923	*P.aeruginosa* ATCC27853	*S. pyogen* ATCC19615
Fe_3O_4 (1:2)	A1 50 µg/ml	8	9	8	8
	A2 75 µg/ml	10	11	9	10
	A3 100 µg/ml	11	12	10	11
	Ampicillin (+ve control)	12	13	12	13.5

5. CONCLUSION AND RECOMMENDATIONS

5.1 Conclusion

A study to evaluate the adsorption efficiency of magnetite nanoparticles in removing Cr(VI) ions from an aqueous solution and also to investigate the antibacterial activity of magnetite nanoparticles. Magnetite nanoparticles were synthesized via the green method by using *Catha edulis* plant leaf extract as a reducing and capping agent. The XRD study showed that the Fe_3O_4 NPs were cubic face-centered with an average crystallite size between 9 and 12 nm. FTIR studies where confirmed the reduction of Fe_3O_4 NPs by active metabolites found in plant leaf extract and the formation of the nanoparticle by the green synthesis method. UV-Vis DRS showed that the formation of magnetite nanoparticles had promoted the adsorption in a visible area. Different morphologies and microstructural characteristics of Fe_3O_4 NPs were shown by the SEM image. A batch adsorption experiment was used to investigate the efficiency of adsorbent for different parameters such as pH, initial concentration; adsorbent dose and contact time have been studied at room temperature. The adsorption of chromium (VI) by Fe_3O_4 NPs was highly pH-sensitive. Optimum parameters pH 5, dose 1g, concentration 20(mg/L), and contact time 60min were obtained. Regarding the adsorption process, Fe_3O_4 NPs sorption was well described by the Freundlich adsorption isotherm. In addition, Pseudo-second Order Kinetic Model best represent adsorption kinetics: therefore it is possible to identify the surface adsorption of ion as the rate-limiting step during the Chemisorption. The synthesized nanomaterials (Fe_3O_4 NPs) have exhibited very good reusability after four cycles. Removal of hexavalent chromium is therefore effectively performed using adsorption on magnetite nanoparticles. In addition, Fe_3O_4 NPs evaluated for antibacterial activity test by the disk diffusion method against two gram-positive (*S. aureus and S. pyogen*) bacteria and two gram-negative (*E. coli and P. aeruginosa*) bacteria. Furthermore, magnetite nanoparticle has potential application in antibacterial activity owing to it is small size with a specific surface area

5.2 Recommendation

Based on the present finding of Fe_3O_4 NPs synthesized by using *Catha edulis* plant leaf extract for chromium adsorption and antibacterial activity, the following recommendations are forwarded to benefit those who want to focus on this area of study the result of the study under consideration.

- ✓ Since hexavalent chromium was removed from the aqueous solution in the present study. Further studies can be done on chromium removal from wastewater effluent
- ✓ The adsorbent could be tested for other toxic heavy metal removal efficiency.
- ✓ The antibacterial studies can be extended to other bacteria strain

REFERENCES

Abate, G. Y., Alene, A. N., Habte, A. T., & Getahun, D. M. (2020). Adsorptive removal of malachite green dye from aqueous solution onto activated carbon of *Catha edulis* stem as a low cost bio-adsorbent. *Environmental Systems Research*, *9*(1). https://doi.org/10.1186/s40068-020-00191-4

Ali, A., & Ahmed, S. (2018). *Green Synthesis of Metal , Metal Oxide Nanoparticles , and Their Various Applications*.

Altaf, S., Zafar, R., Zaman, W. Q., Ahmad, S., Yaqoob, K., Syed, A., Khan, A. J., Bilal, M., & Arshad, M. (2021). Removal of levofloxacin from aqueous solution by green synthesized magnetite (Fe_3O_4) nanoparticles using *Moringa olifera*: Kinetics and reaction mechanism analysis. *Ecotoxicology and Environmental Safety*, *226*, 112826. https://doi.org/10.1016/j.ecoenv.2021.112826

Andualem, W. W., Sabir, F. K., Mohammed, E. T., Belay, H. H., & Gonfa, B. A. (2020). Synthesis of copper oxide nanoparticles using plant leaf extract of catha edulis and its antibacterial activity. *Journal of Nanotechnology*, *2020*. https://doi.org/10.1155/2020/2932434

Ansari, S. A., Oves, M., Satar, R., Khan, A., Ahmad, S. I., Jafri, M. A., Zaidi, S. K., & Alqahtani, M. H. (2017). Antibacterial activity of iron oxide nanoparticles synthesized by co-precipitation technology against *Bacillus cereus* and *Klebsiella pneumoniae*. *Polish Journal of Chemical Technology*, *19*(4), 110–115. https://doi.org/10.1515/pjct-2017-0076

Anwar, S. H. (2018). *A Brief Review on Nanoparticles : Types of Platforms , Biological Synthesis and Applications*. *6*(2), 109–116. https://doi.org/10.4172/2321-6212.1000222

Aragaw, T. A., Bogale, F. M., & Aragaw, B. A. (2021). Iron-based nanoparticles in wastewater treatment: A review on synthesis methods, applications, and removal mechanisms. *Journal of Saudi Chemical Society*, *25*(8), 101280. https://doi.org/10.1016/j.jscs.2021.101280

Armbrüster, M., & Cardoso-Gil, R. (2015). Synthesis of supported Ga nanodrops by a bottom-

up route. *Zeitschrift Fur Anorganische Und Allgemeine Chemie*, *641*(8–9), 1453–1458. https://doi.org/10.1002/zaac.201500155

Article, O. (2006). *Metal oxide nanoparticles : synthesis , characterization and*. 161–164. https://doi.org/10.1007/s10971-005-6621-2

Asab, G., Zereffa, E. A., & Abdo Seghne, T. (2020). Synthesis of Silica-Coated Fe_3O_4 Nanoparticles by Microemulsion Method: Characterization and Evaluation of Antimicrobial Activity. *International Journal of Biomaterials*, *2020*. https://doi.org/10.1155/2020/4783612

Asfaw, G. (2021). *Green Synthesis of Fe $_3$ O $_4$ Nanoparticles Using Eucalyptus Globules Leaf Extract and Its Application for Phosphate Removal from Synthetic Wastewater*. Unpublished" MSc. Thesis Submitted to Adama science and Technology University, 39 pp. *August*.

Assefa, T., & Mazengiaw, F. (2021). Iron-based nanoparticles in wastewater treatment : A review on synthesis methods , applications , and removal mechanisms. *Journal of Saudi Chemical Society*, *25*(8), 101280. https://doi.org/10.1016/j.jscs.2021.101280

Ayawei, N., Ebelegi, A. N., & Wankasi, D. (2017). *Modelling and Interpretation of Adsorption Isotherms*. *2017*.

Behera, S. S., Patra, J. K., Pramanik, K., Panda, N., & Thatoi, H. (2012). Characterization and Evaluation of Antibacterial Activities of Chemically Synthesized Iron Oxide Nanoparticles. *World Journal of Nano Science and Engineering*, *02*(04), 196–200. https://doi.org/10.4236/wjnse.2012.24026

Beyan, S. M., Prabhu, S. V., Ambio, T. A., & Gomadurai, C. (2022). *Research Article A Statistical Modeling and Optimization for Cr (VI) Adsorption from Aqueous Media via Teff Straw-Based Activated Carbon : Isotherm , Kinetics , and Thermodynamic Studies*. *2022*(Vi).

Bolade, O. P., Williams, A. B., & Benson, N. U. (2019). na l P of. *Environmental Nanotechnology, Monitoring & Management*, 100279.

https://doi.org/10.1016/j.enmm.2019.100279

Bolade, O. P., Williams, A. B., & Benson, N. U. (2020). Green synthesis of iron-based nanomaterials for environmental remediation: A review. *Environmental Nanotechnology, Monitoring and Management*, *13*(February 2019). https://doi.org/10.1016/j.enmm.2019.100279

Borja, J. Q., Ngo, M. A. S., Saranglao, C. C., Tiongco, R. P. M., Roque, E. C., & Dugos, N. P. (2015). Synthesis of green zero-valent iron using polyphenols from dried green tea extract. *Journal of Engineering Science and Technology*, *10*(Spec.issue7), 22–31.

Chen, Y. G., Ye, W. M., Yang, X. M., Deng, F. Y., & He, Y. (2011). Effect of contact time, pH, and ionic strength on Cd(II) adsorption from aqueous solution onto bentonite from Gaomiaozi, China. *Environmental Earth Sciences*, *64*(2), 329–336. https://doi.org/10.1007/s12665-010-0850-6

Çiftçi, H., Ersoy, B., & Evcin, A. (2017). *Synthesis , Characterization and Cr (VI) Adsorption Properties of Modified Magnetite Nanoparticles*. *132*(3), 564–569. https://doi.org/10.12693/APhysPolA.132.564

Dhal, B., Abhilash, & Pandey, B. D. (2018). Mechanism elucidation and adsorbent characterization for removal of Cr(VI) by native fungal adsorbent. *Sustainable Environment Research*, *28*(6), 289–297. https://doi.org/10.1016/j.serj.2018.05.002

Dhar, P. K., Saha, P., Hasan, M. K., Amin, M. K., & Haque, M. R. (2021). Green synthesis of magnetite nanoparticles using Lathyrus sativus peel extract and evaluation of their catalytic activity. Clean Eng. and Technol. 3: 100117.

Edris, J., Gupta, N., & Zereffa, E. A. (2019). Synthesis of Silica Supported Iron Oxide Nanoparticles for Hexavalent Chromium Removal from Aqueous Solutions. *Ethiopian Journal of Sciences and Sustainable Development*, *6*(2), 81–93.

El-Sheikh, A. H., Fasfous, I. I., Al-Salamin, R. M., & Newman, A. P. (2018). Immobilization of citric acid and magnetite on sawdust for competitive adsorption and extraction of metal ions from environmental waters. *Journal of Environmental Chemical Engineering*,

6(4), 5186–5195. https://doi.org/10.1016/j.jece.2018.08.020

Gabal, R. A., Shokeir, D., & Orabi, A. (2022). *Cytotoxicity and Hemostatic One Step Green Synthesis of Iron Nanoparticles Coated with Green Tea for Biomedical Application*.*Trend in science*. *19*(3).

Gebeyehu, H. R., Danno, L., & Id, B. (2020). *Levels of heavy metals in soil and vegetables and associated health risks in Mojo area ,journal plos org*. 1–22.

Geneti, S. T., Mekonnen, G. A., Murthy, H. C. A., Mohammed, E. T., Ravikumar, C. R., Gonfa, B. A., & Sabir, F. K. (2022). *Biogenic Synthesis of Magnetite Nanoparticles Using Leaf Extract of Thymus schimperi and Their Application for Monocomponent Removal of Chromium and Mercury Ions from Aqueous Solution journal of chemistry. 2022*(3).

Getasetegn, M. (2016). Chemical composition of Catha edulis (khat): a review. *Phytochemistry Reviews*, *15*(5), 907–920. https://doi.org/10.1007/s11101-015-9435-z

Hajba, L., & Guttman, A. (2016). The use of magnetic nanoparticles in cancer theranostics: Toward handheld diagnostic devices. *Biotechnology Advances*, *34*(4), 354–361. https://doi.org/10.1016/j.biotechadv.2016.02.001

Husk, C. (2017). *Journal of Material Sciences & Engineering Removal of Chromium from Industrial Wastewater by Adsorption Using*. *6*(2), 6–11. https://doi.org/10.4172/2169-0022.1000331

Jadidi, M., Etesami, N., & Esfahany, M. N. (2017). *Adsorption and Desorption Processes of Chromium Ions Using Magnetic Iron Oxide Nanoparticles and Their Relevant Mechanism*. *14*(3), 31–40.

Jain, K., Patel, A. S., Pardhi, V. P., & Flora, J. S. S. (2021). Nanotechnology in Wastewater Management : A New Paradigm. *Molecules*, *26*, 1797.

Khatami, M., Aflatoonian, M. R., Azizi, H., Mosazade, F., Hooshmand, A., Lima Nobre, M. A., Minab Poodineh, F., Khatami, M., Khraazi, S., & Mirzaeei, H. (2017). Evaluation of Antibacterial Activity of Iron Oxide Nanoparticles Against Escherichia coli.

International Journal of Basic Science in Medicine, *2*(4), 166–169. https://doi.org/10.15171/ijbsm.2017.31

Kiflom Gebremedhn, Mebrahtu Hagos Kahsay, & Muluken Aklilu. (2019). Green Synthesis of CuO Nanoparticles Using Leaf Extract of *Catha edulis* and Its Antibacterial Activity. *Journal of Pharmacy and Pharmacology*, *7*(6). https://doi.org/10.17265/2328-2150/2019.06.007

Kumar, V. (2019). *Green Synthesis and Characterization of Iron Oxide Nanoparticles Using Phyllanthus Niruri Extract*.

Kumavat, S. R., & Mishra, S. (2021). Green synthesis of silver nanoparticles using Borago officinalis leaves extract and screening its antimicrobial and antifungal activity. *International Nano Letters*, *11*(4), 355–370. https://doi.org/10.1007/s40089-021-00345-x

Liu, G., Gao, J., Ai, H., & Chen, X. (2013). *Applications and Potential Toxicity of Magnetic Iron Oxide Nanoparticles*. *9*, 1533–1545. https://doi.org/10.1002/smll.201201531

Mahdavi, M., Namvar, F., Ahmad, M. Bin, & Mohamad, R. (2013). *Green Biosynthesis and Characterization of Magnetic Iron Oxide (Fe_3O_4) Nanoparticles Using Seaweed (Sargassum muticum) Aqueous Extract*. 5954–5964. https://doi.org/10.3390/molecules18055954

Manandhar, S., Luitel, S., & Dahal, R. K. (2019). In Vitro Antimicrobial Activity of Some Medicinal Plants against Human Pathogenic Bacteria. *Journal of Tropical Medicine*, *2019*. https://doi.org/10.1155/2019/1895340

Marcu, C., Varodi, C., & Balla, A. (2020). Adsorption Kinetics of Chromium (VI) from Aqueous Solution Using an Anion Exchange Resin Solution Using an Anion Exchange Resin. *Analytical Letters*, *0*(0), 1–10. https://doi.org/10.1080/00032719.2020.1731523

Michael, S., Solomon, K., & Omoniyi, A. (2020). *Short Review Article Plant-Mediated Iron Nanoparticles and their Applications as Adsorbents for Water Treatment – A Review*. *2*(2), 103–113. https://doi.org/10.33945/SAMI/JCR.2020.2.3

Microbes, P. (2016). *Nanoparticles : Alternatives Against Drug-Resistant*. 1–30.

https://doi.org/10.3390/molecules21070836

Moussout, H., Ahlafi, H., Aazza, M., & Maghat, H. (2018). ScienceDirect Critical of linear and nonlinear equations of pseudo-first order and pseudo-second order kinetic models. *Karbala International Journal of Modern Science*. https://doi.org/10.1016/j.kijoms.2018.04.001

Mukherjee, P. (2017). Stenotrophomonas and Microbacterium: Mediated Biogenesis of Copper, Silver and Iron Nanoparticles—Proteomic Insights and Antibacterial Properties Versus Biofilm Formation. *Journal of Cluster Science*, *28*(1), 331–358. https://doi.org/10.1007/s10876-016-1097-5

Mulu, A., Ayenew, T., & Berhe, S. (2015). *Impact of Slaughterhouses Effluent on Water Quality of Modjo and Akaki River in Central Ethiopia*. *April*.

Namdeo, M. (2018). Magnetite Nanoparticles as Effective Adsorbent for Water Purification-A Review. *Advances in Recycling & Waste Management*, *02*(03). https://doi.org/10.4172/2475-7675.1000135

Nameni, M., Moghadam, M. R. A., & Arami, M. (n.d.). *Archive of SID Adsorption of hexavalent chromium from aqueous solutions by wheat bran*.

Nanoliposomes, E. R. (2013). *Nanoparticles as Drug Delivery Systems in Cancer Medicine :* 1361–1380. https://doi.org/10.3390/ph6111361

Padmavathy, K. S., Madhu, G., & Haseena, P. V. (2016). A study on Effects of pH, Adsorbent Dosage, Time, Initial Concentration and Adsorption Isotherm Study for the Removal of Hexavalent Chromium (Cr (VI)) from Wastewater by Magnetite Nanoparticles. *Procedia Technology*, *24*, 585–594. https://doi.org/10.1016/j.protcy.2016.05.127

Pandey, P. K., Sharma, S. K., & Sambi, S. S. (2010). *Archive of SID*. *7*(2), 395–404.

Pessan, J. P., Paula, A., Vieira, M., Maria, T., Lima, T. De, Carlos, A., & Delbem, B. (2018). *Iron Oxide Nanoparticles for Biomedical Applications : A Perspective on Synthesis , Drugs , Antimicrobial Activity , and Toxicity*. https://doi.org/10.3390/antibiotics7020046

Pitchay, T., Jawad, A. H., Johari, I. S., & Sabar, S. (2022). Kinetics Studies of Metallic Ions Adsorption by Immobilised Chitosan. *Science Letters*, *16*(1), 137. https://doi.org/10.24191/sl.v16i1.15932

Rajput, S., Pittman, C. U., & Mohan, D. (2016). Magnetic magnetite (Fe_3O_4) nanoparticle synthesis and applications for lead (Pb^{2+}) and chromium (Cr^{6+}) removal from water. *Journal of Colloid and Interface Science*, *468*, 334–346. https://doi.org/10.1016/j.jcis.2015.12.008

Sallak, N., Moghanjoughi, A. M., & Ataee, M. (n.d.). *Antimicrobial biodegradable fi lm based on corn starch / Satureja khuzestanica essential oil / Ag – TiO 2 nanocomposites*.

Sathishkumar, G., Logeshwaran, V., Sarathbabu, S., Jha, P. K., Jeyaraj, M., Rajkuberan, C., Senthilkumar, N., & Sivaramakrishnan, S. (2018). Green synthesis of magnetic Fe_3O_4 nanoparticles using Couroupita guianensis Aubl. fruit extract for their antibacterial and cytotoxicity activities. *Artificial Cells, Nanomedicine and Biotechnology*, *46*(3), 589–598. https://doi.org/10.1080/21691401.2017.1332635

Sathya, K., Saravanathamizhan, R., & Baskar, G. (2018). *ReView by River Valley This Technologies IET Nanobiotechnology Green Synthesized Iron and Iron Based Nanoparticle in Environmental and Biomedical Application – A Review IET Review Copy Only ReView by River Valley This Technologies IET Nanobiotechnology ar*. 2–15.

Sepasgozar, S. M. E., Feizyzadeh, B., Morsali, A., Branch, Q., Branch, Q., & Branch, M. (2022). *Eco-Friendly Synthesis of Magnetic Iron Oxide Nanoparticles Using Achillea Nobilis Extract and Evaluation of Their Antioxidant and Antibacterial properties*. *12*(2), 61–71. https://doi.org/10.30495/JFBT.2022.19330

Sheshmani, S., & Mashhadi, S. (2018). Potential of magnetite reduced graphene oxide/chitosan nanocomposite as biosorbent for the removal of dyes from aqueous solutions. *Polymer Composites*, *39*, E457–E462. https://doi.org/10.1002/pc.24608

Singh, M., Goyal, M., & Devlal, K. (2018). Size and shape effects on the band gap of semiconductor compound nanomaterials. *Journal of Taibah University for Science*, *12*(4), 470–475. https://doi.org/10.1080/16583655.2018.1473946

Singh, R., & Bhateria, R. (2020). Optimization and experimental design of the Pb^{2+}adsorption process on a nano-Fe_3O_4-based adsorbent using the response surface methodology. *ACS Omega*, *5*(43), 28305–28318. https://doi.org/10.1021/acsomega.0c04284

Singh, R., & Nalwa, H. S. (2011). *Medical Applications of Nanoparticles in Biological Imaging , Cell Labeling , Antimicrobial Agents , and Anticancer Nanodrugs*. *Journal of biomedical nanotechnology*, *7*(4), 489–503. https://doi.org/10.1166/jbn.2011.1324

Smuleac, V., Varma, R., Baruwati, B., Sikdar, S., & Bhattacharyya, D. (2011). Nanostructured membranes for enzyme catalysis and green synthesis of nanoparticles. *ChemSusChem*, *4*(12), 1773–1777. https://doi.org/10.1002/cssc.201100211

Taimoory, S. M., Rahdar, A., Aliahmad, M., Sadeghfar, F., Hajinezhad, M. R., Jahantigh, M., Shahbazi, P., & Trant, J. F. (2018). The synthesis and characterization of a magnetite nanoparticle with potent antibacterial activity and low mammalian toxicity. *Journal of Molecular Liquids*, *265*(2017), 96–104. https://doi.org/10.1016/j.molliq.2018.05.105

Wahid, F., Zhong, C., Wang, H. S., Hu, X. H., & Chu, L. Q. (2017). Recent advances in antimicrobial hydrogels containing metal ions and metals/metal oxide nanoparticles. *Polymers*, *9*(12). https://doi.org/10.3390/polym9120636

Weijiang, Z., Yace, Z., Yuvaraja, G., & Jiao, X. (2017). Adsorption of Pb(II) ions from aqueous environment using eco-friendly chitosan schiff's base@Fe_3O_4 (CSB@Fe_3O_4) as an adsorbent; kinetics, isotherm and thermodynamic studies. *International Journal of Biological Macromolecules*, *4*(Ii). https://doi.org/10.1016/j.ijbiomac.2017.07.063

Wu, S., Sun, A., Zhai, F., Wang, J., Xu, W., Zhang, Q., & Volinsky, A. A. (2011). Fe_3O_4 magnetic nanoparticles synthesis from tailings by ultrasonic chemical co-precipitation. *Materials Letters*, *65*(12), 1882–1884. https://doi.org/10.1016/j.matlet.2011.03.065

Wu, W., He, Q., & Jiang, C. (2008). Magnetic iron oxide nanoparticles: Synthesis and surface functionalization strategies. *Nanoscale Research Letters*, *3*(11), 397–415. https://doi.org/10.1007/s11671-008-9174-9

Yew, Y. P., Shameli, K., Miyake, M., Kuwano, N., Bt Ahmad Khairudin, N. B., Bt Mohamad,

S. E., & Lee, K. X. (2016). Green Synthesis of Magnetite (Fe_3O_4) Nanoparticles Using Seaweed (Kappaphycus alvarezii) Extract. *Nanoscale Research Letters*, *11*(1). https://doi.org/10.1186/s11671-016-1498-2

Yuan, P., Liu, D., Fan, M., Yang, D., Zhu, R., Ge, F., Zhu, J. X., & He, H. (2010). Removal of hexavalent chromium [Cr(VI)] from aqueous solutions by the diatomite-supported/unsupported magnetite nanoparticles. *Journal of Hazardous Materials*, *173*(1–3), 614–621. https://doi.org/10.1016/j.jhazmat.2009.08.129

Yusefi, M., Shameli, K., Hedayatnasab, Z., & Yeang, S. (2021). Green synthesis of Fe_3O_4 nanoparticles for hyperthermia, magnetic resonance imaging and 5-fluorouracil carrier in potential colorectal cancer treatment. *Research on Chemical Intermediates*, *47*(5), 1789–1808. https://doi.org/10.1007/s11164-020-04388-1

Zhang, X. F., Liu, Z. G., Shen, W., & Gurunathan, S. (2016). Silver nanoparticles: Synthesis, characterization, properties, applications, and therapeutic approaches. *International Journal of Molecular Sciences*, *17*(9). https://doi.org/10.3390/ijms17091534

APPENDIXES

Table 7: Percent removal of hexavalent chromium from aqueous solution by using different ratio of Fe_3O_4 NPs

Fe_3O_4 NPs ratios	Initial conc. (mg/L)	Equilibrium Absorbance (C_e)	C_e	Average final conc. (mg/L)	Removal efficiency
1:1 Fe_3O_4 NPs	20mg/L	0.0627	0.545	0.18685	97.2%
2:1 Fe_3O_4 NPs	20mg/L	0.0683	0.61	0.35	96.9%
1:2 Fe_3O_4 NPs	20mg/L	0.046	0.35	0.11678	98.2%

Table 8: The effect of pH on the adsorptive removal of Cr(VI) from aqueous solution

pH	Initial Cr(VI) Conc. (mg/L)	Final Cr(VI) Conc. (mg/L)	Removal Efficiency (%
3	20	3.912	80.4
5	20	0.3	98.4
7	20	1.716	91.4
9	20	2.1	89.5
11	20	4.7	76.3

Table 9: The effect of adsorbent dose on the adsorptive removal of Cr(VI) from aqueous solution

Adsorbent dose (mg)	Initial Cr(VI) Conc. (mg/L)	Final Cr(VI) Conc. (mg/L)	Removal Efficiency (%
250	20	4.9	75.4
500	20	1.389	93
750	20	1.249	93.7
1000	20	0.327	98.3
1250	20	0.278	98.6

Table 10: The effect of contact time on the adsorptive removal of hexavalent chromium ion from aqueous solution

Contact time (min)	Initial Cr(VI) Conc. (mg/L)	Final Cr(VI) Conc. (mg/L)	Removal Efficiency (%
20	30	6.995	76.6
40	30	4.91	83.6
60	30	1.167	96.1
80	30	1.389	95.3
100	30	1.47	95

Table 11: The effect of initial concentration on the adsorptive removal of Cr(VI) from aqueous solution

initial concentration (mg/L)	Final Cr(VI) Conc. (mg/L)	Removal Efficiency (%
20	0.03987	98.6
30	3.223	89.2
40	7.07	82.3
50	14.41	71.2
60	21.1	64.8

Table 12: experimental and calculated data for pseudo first order model

Experiment number	time(min)	C_i (mg/L)	C_e(mg/L)	q_t(mg/g)	ln(qe-qt)
1	0	0	0	0	0
2	20	20	6.99	2.168333	0.1030589
3	40	20	4.9	2.516667	-0.274143
4	60	20	1.167	3.138833	-1.9800911
5	80	20	1.389	3.101833	-1.7426455

6	100	20	1.47	3.088333	-1.6683567

Table 13: experimental and calculated data for pseudo second order model

time(min)	C_i(mg/L)	C_e(mg/L)	q_t(mg/g)	t/qt
0	0	0	0	0
20	20	6.99	2.168333	9.2236741
40	20	4.9	2.516667	15.89404
60	20	1.167	3.138833	19.115383
80	20	1.389	3.101833	25.791199
100	20	1.47	3.088333	32.379924

Table 14: experimental and calculated data for Freundlich isotherm

expt no	Ci(mg/L)	C_e (mg/L)	$1/C_e$	log C_e	ln Ce	q_e(mg/g)	$1/q_e$	log q_e
1	20	0.33866	2.952814	-0.47024	-1.08276	3.27689	0.3051	0.515461
2	30	3.22	0.310559	0.5078	1.16938	4.46333	0.22404	0.649659
3	40	7.07	0.141443	0.84941	1.95586	5.48833	0.18220	0.739440
4	50	14.4	0.069444	1.15836	2.66722	5.93333	0.16853	0.773298
5	60	21.1	0.047393	1.32428	3.04927	6.48333	0.154242	0.8117984

Table 15: experimental and calculated data for Langmuir isotherm

expt no	C_i(mg/L)	C_e (mg/L)	$1/c_e$	log c_e	ln C_e	q_e(mg/g)	$1/q_e$	log q_e
1	20	0.33866	2.952814	-0.47024	-1.08276	3.27689	0.305167	0.5154619
2	30	3.22	0.310559	0.507856	1.169381	4.463333	0.224048	0.6496593
3	40	7.07	0.141443	0.849419	1.95586	5.488333	0.182205	0.7394405
4	50	14.4	0.069444	1.158362	2.667228	5.933333	0.168539	0.7732987
5	60	21.1	0.047393	1.324282	3.049273	6.483333	0.154242	0.8117984

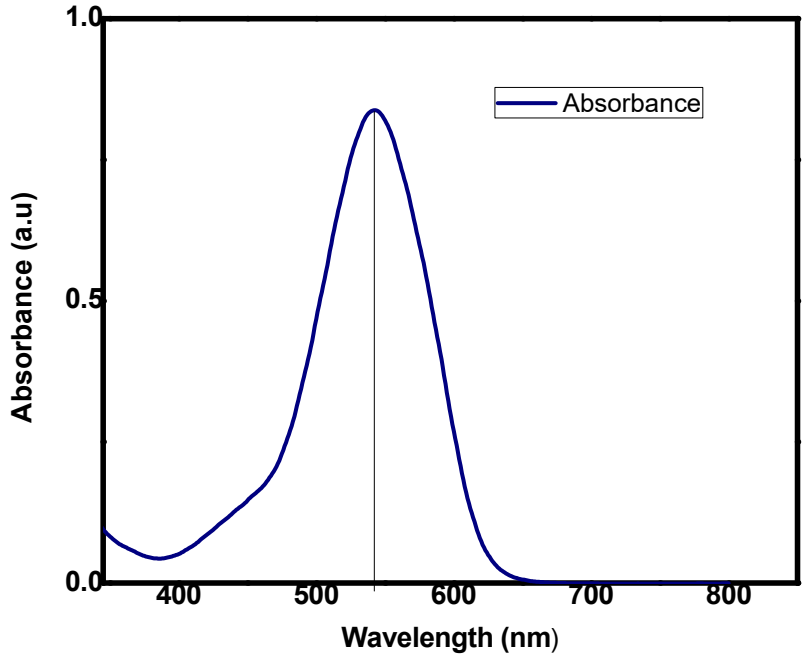

Figure 27 UV-Visible ʎ maximum absorption of Chromium (VI)

Some selected figure during laboratory work

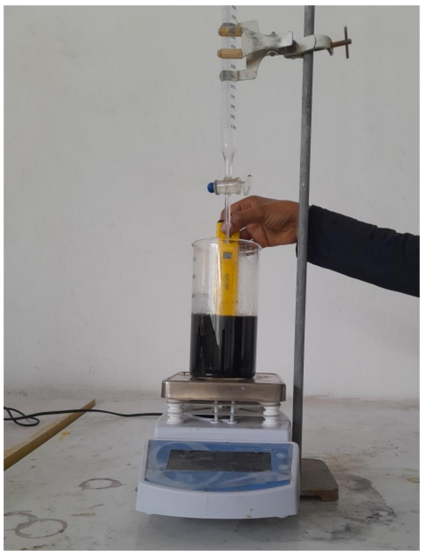

Figure 28: pH adjustment during synthesis of nanoparticle

Figure 29: initial concentration of chromium solution which is used during adsorption experiment

Figure 30: Sample ready for measurement after 1, 5diphenyl carbazide added Laboratory

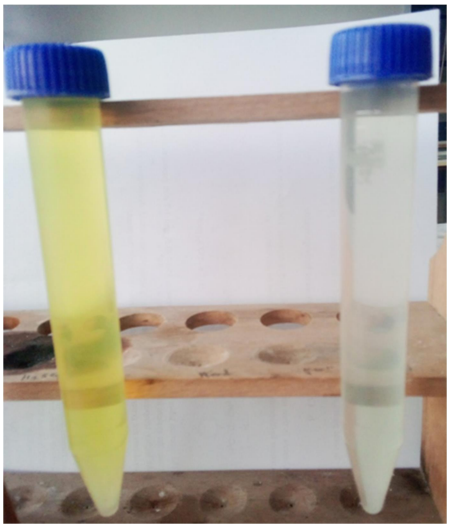

Figure 31: Chromium containing solution before and after treatment at pH = 5, adsorbent dose = 1 g/100ml and chromium concentration = 20 mg/l.